

1 **Surface-Shaving Proteomics of *Mycobacterium marinum* Identifies**
2 **Biofilm Subtype-Specific Changes Affecting Virulence, Tolerance and**
3 **Persistence**

4
5 **Kirsi Savijoki^{a*}, Henna Myllymäki^{b*,**}, Hanna Luukinen^b, Lauri Paulamäki^b,**
6 **Leena-Maija Vanha-aho^b, Aleksandra Svorjova^b, Ilkka Miettinen^a, Adyary**
7 **Fallarero^{a,***}, Teemu O. Ihalainen^b, Jari Yli-Kauhaluoma^d, Tuula A. Nyman^d,**
8 **Mataleena Parikka^{b#}**

9
10 a) Drug Research Program, Division of Pharmaceutical Biosciences, Faculty of
11 Pharmacy, FI-00014, University of Helsinki, Finland

12 b) Faculty of Medicine and Health Technology, FI-33014
13 Tampere University, Finland

14 c) Drug Research Program, Division of Pharmaceutical Chemistry and Technology,
15 Faculty of Pharmacy, University of Helsinki, FI-00014, Finland

16 d) Institute of Clinical Medicine, Department of Immunology, Faculty of Medicine,
17 Rikshospitalet, University of Oslo and Oslo University Hospital, Norway

18
19 **# Correspondence to: Mataleena Parikka**

20 Email: mataleena.parikka@tuni.fi

21 Tel: +358 40 735 5052

22
23 *** These authors contributed equally to this work**

24 **** Current address: UoE Centre for Inflammation Research, Queen's Medical**
25 **Research Institute, University of Edinburgh, United Kingdom**

26 ***** Current address: Thermo Fischer Scientific, Ratastie 2, 01620 Vantaa, Finland**

27
28 **Running title: *Mycobacterium marinum* cell-surface proteome profiling**

29

30 **ABSTRACT (250 words)**

31 The complex cell wall and biofilm matrix (ECM) act as key barriers to antibiotics in
32 mycobacteria. Here, the ECM-proteins of *Mycobacterium marinum* ATCC927, a non-
33 tuberculous mycobacterial model, was monitored over three months by label-free
34 proteomics and compared with cell-surface proteins on planktonic cells to uncover
35 pathways leading to virulence, tolerance, and persistence. We show that ATCC927 forms
36 pellicle-type (PBFs) and submerged-type (SBFs) biofilms after two weeks and two days of
37 growth, respectively, and that the increased CelA1 synthesis in this strain prevents biofilm
38 formation and leads to reduced rifampicin tolerance. The proteomic data suggests that
39 specific changes in mycolic acid synthesis (cord factor), Esx1-secretion, and cell-wall
40 adhesins explain the appearance of PBFs as ribbon-like cords and SBFs as lichen-like
41 structures. A subpopulation of cells resisting the $64 \times$ MIC rifampicin (persisters) were
42 detected in both biofilm subtypes, and already in one-week-old SBFs. The key forces
43 boosting their development could include subtype-dependent changes in asymmetric cell
44 division, cell wall biogenesis, tricarboxylic acid/glyoxylate cycle activities, and
45 energy/redox/iron metabolisms. The effect of varying ambient oxygen tensions on each
46 cell type and non-classical protein secretion are likely factors explaining majority of the
47 subtype-specific changes. The proteomic findings also imply that Esx1-type protein
48 secretion is more efficient in PL and PBF cells, while SBF may prefer both the Esx5- and
49 non-classical pathways to control virulence and prolonged viability/persistence. In
50 conclusion, this study reports a first proteomic insight into aging mycobacterial biofilm-
51 ECMs and indicates biofilm subtype-dependent mechanisms conferring increased
52 adaptive potential and virulence on non-tuberculous mycobacteria.

53

54 **IMPORTANCE (88 words)**

55 Mycobacteria are naturally resilient and mycobacterial infections are notoriously difficult to
56 treat with antibiotics, with biofilm formation being the main factor complicating the
57 successful treatment of TB. The present study shows that non-tuberculous *Mycobacterium*
58 *marinum* ATCC927 forms submerged- and pellicle-type biofilms with lichen- and ribbon-
59 like structures, respectively, as well as persister cells under the same conditions. We show
60 that both biofilm subtypes differ in terms of virulence-, tolerance- and persistence-
61 conferring activities, highlighting the fact that both subtypes should be targeted to
62 maximize the power of antimycobacterial treatment therapies.

63

64 **INTRODUCTION (5735 words)**

65 Tuberculosis (TB) remains a major global health issue, with approximately 10 million new
66 cases and 1.4 million deaths in 2019 (1). The causative agent, *Mycobacterium*
67 *tuberculosis* (Mtb), is carried by an estimated one quarter of the human population as a
68 latent infection, which has a 5–10% lifetime risk of developing into TB disease. In addition,
69 the emergence of drug-resistant Mtb strains continues to be a public health threat, with
70 about half a million new cases in 2019. Even in the case of drug-sensitive Mtb strains, the
71 first line antibiotic treatment requires the use of four antimicrobials over a course of at least
72 six months (WHO 2020). Moreover, despite successful treatment, the recurrence of TB
73 carries a substantial risk, especially among immunocompromised patients (2, 3). The
74 heterogeneity of the standard treatment outcome is also evident in PET-CT images
75 showing non-resolving and active lesions and the presence of Mtb mRNA in sputum
76 samples. This suggests that a significant proportion of patients generate viable
77 mycobacteria in their lungs even after clinically curative antibiotic treatment (4). In a rabbit
78 TB model, it was further shown that the caseum of granulomas contains Mtb that are

79 highly tolerant to most anti-TB drugs (5). The complex mycobacterial cell wall, involving
80 capsule and outer/inner membranes connected by a dense mycolyl-arabinogalactan-
81 peptidoglycan with high lipid levels, is the main barrier that protects the bacterial cells
82 against drugs (6). While the mechanisms leading to drug tolerance in TB have remained
83 poorly understood, biofilm formation was recently indicated as one of the strategies to
84 increase viability, tolerance and persistence (7-10).

85 Biofilm formation is defined as adherent growth within self-produced extracellular
86 matrix/ECM consisting of proteins, polysaccharides, and DNA/RNA, and it is the strategy
87 bacteria use to escape the effects of antibiotics and host defense systems (11-13).
88 Mycobacteria use phenotypically distinct biofilm subtypes for growth, which genetically and
89 physiologically differ from the planktonic-type growth. These include (i) floating/pellicle-
90 type biofilms (PBFs) at the air-liquid interface having an ECM rich in free mycolic acids
91 (MAs) and with a frequent cord/ribbon-like appearance, while (ii) submerged-type biofilms
92 (SBFs) show adherent growth on a solid substratum (11, 14-16). The capsule layer plays a
93 vital role in triggering biofilm growth in mycobacteria, as cells cultured in the presence of
94 Tween-80 (non-ionic surfactant) has been shown to detach the capsule layer and prevent
95 the biofilm formation (17). Thus, this labile layer forming the first molecular interaction with
96 the host/environment is likely to involve key factors contributing to persistence/adaptation
97 and search of anti-TB targets. Although several studies on mycobacteria have pinpointed
98 cellular pathways and proteins that affect the capsule/cell wall and the biofilm formation (9,
99 14, 17-25), systematic investigation of the factors that directly interact with the surrounding
100 environment is necessary to be able to maximize the power of antimycobacterial treatment
101 therapies.

102 *Mycobacterium marinum* (Mmr) has proven to be an excellent alternative model pathogen
103 for slow-growing Mtb, as it allows for the investigation of TB-like chronic and latent

104 infections in its natural host, the zebrafish (26-29). Cultured mycobacterial biofilms have
105 been used to understand resilient bacterial phenotypes emerging in mycobacterial
106 infections. However, the distinct phenotypic profiles associated with PBFs and SBFs,
107 including marker proteins discriminating the two biofilm subtypes have remained poorly
108 understood. To shed light on the specific attributes linking these biologically different
109 biofilm subtypes to their phenotypes, we first cultured Mmr strain ATCC927 to create in
110 vitro biofilms. These biofilms were then imaged using widefield deconvolution microscopy
111 (WDeM) to investigate temporal effects on the biofilm architectures. Label-free quantitative
112 (LFQ) proteomics was next used to uncover the ECM-proteome dynamics in maturing Mmr
113 biofilms and to identify the cell surface proteins (proteome) on Mmr grown on Tween-80, a
114 detergent known to prevent cells from clumping and forming a biofilm (17). The key
115 proteome findings were validated by gene overexpression studies to indicate cellulose-
116 dependent biofilm formation as well as biofilm killing assays to confirm the formation of
117 persister cells in both biofilm subtypes. To the best of our knowledge, this is the first study
118 monitoring mycobacterial ECM-proteomes over three months' time as well as protein and
119 morphological phenotypic markers for distinguishing defined biofilm subtypes.

120

121 **RESULTS**

122 **SBFs and PBFs show distinct morphological characteristics**

123 The kinetics of development and maturation as well as the morphology of mycobacterial
124 PBFs and SBFs has been reported to differ substantially (8). Here, we first show that that
125 Mmr forms PBFs at the air-liquid interphase and SBFs attached onto the bottom of the
126 culture well under the same physiological in vitro conditions after two weeks of growth
127 **(Fig. 1SA)**. The SBF subtype develops earlier (visible already after two days of culture)
128 than the PBF, which was not clearly distinguishable before two weeks of growth. Next, we

129 investigated the three-dimensional morphology of Mmr biofilms in more detail by culturing
130 Mmr cells, carrying the pTEC27 plasmid with the tdTomato fluorescent marker gene (29),
131 for two and three weeks to produce PBFs and SBFs, and analyzing the biofilms by
132 widefield deconvolution microscopy (WDeM). **Figure 1** shows that Mmr forms organized,
133 three-dimensional structures with distinctive, subtype-specific morphological features. For
134 the SBF, the structures displayed a lichen- or moss-like appearance, having tens of
135 microns high feature structures rising from the biofilm base after two weeks (**Fig. 1B**). In
136 comparison, the morphology of the PBF subtype was very different by the first time point,
137 showing flat, ribbon-like structures without any protruding structures (**Fig. 1C**). Defined,
138 extensive structures in all dimensions, although less dense compared to those detected at
139 the two-week-time point, were found for both biofilm subtypes also after three weeks of
140 growth.

141

142 **Submerged biofilms exhibit the greatest ECM-proteome diversity**

143 As the phenotypic profiles of PBFs and SBFs are clearly different, their ECM-proteomes
144 were next quantitatively monitored and compared during the development and maturation
145 stages. To this end, the PBF and SBF cells at the points in **Figure 2A** were subjected to
146 trypsin/Lys-C digestion as well as LC-MS/MS-based protein identification and LFQ (all
147 data available via PRIDE with identifier PXD02010). Logarithmic state planktonic cells
148 (PL_log), representing single-cell cultures, were obtained by growing the Mmr strain in the
149 presence of Tween-80. The quality of each data set was high: 84.7% of all proteins were
150 identified with at least three or more matching peptides, with an average sequence
151 coverage of approximately 31% and only 11% of proteins were categorized as single-
152 peptide-hits. In addition, a broad overlap in protein identifications was detected within the
153 four biological replica samples; 41-89 % of the proteins were shared by each replicate,

154 with the two-week PBF and the three-week SBF showing the highest variation between
155 replicates (**Fig. S1B**). **Table S1** lists the proteins detected in at least two out of four replica
156 samples. An outlier replicate associated with one of the SBF identification replica sets at
157 the three-week-timepoint was excluded from subsequent data analyses. The number of
158 detected proteins was 1132, 1957, and 2133 for the PL, PBF and SBF cells, respectively.

159

160 **Cytoplasmic protein export/release is most efficient in submerged biofilms**

161 **Figure S2A** shows the distribution of all identified proteins according to their predicted
162 secretion motif (Sec/SPII, TatP/SPI, LIPO/SPII, type VII secretion/T7SS, SecretomeP) and
163 the number of transmembrane spanning domains (TMDs). The most notable differences
164 were detected for membrane proteins with six to ten TMDs as well as in the number of
165 cytoplasmic proteins. Nearly two-fold more TMD proteins were detected in the PL than the
166 biofilm cells. In contrast, two-fold more cytoplasmic proteins predicted to be exported out
167 of the cells via a non-classical route (SecretomeP) were identified from the biofilm-ECMs
168 (n , 300) in comparison to the PL cells (n , 150). For many of these proteins, a secondary
169 function as a moonlighting protein (30) could be indicated (**Table S1**). In addition, over
170 900, 1600 and 1800 cytoplasmic proteins identified on the PL, PBF, and SBF cells,
171 respectively, contained no motifs for classical or non-classical secretion and were
172 assigned here as “Others” (**Table S1**).

173

174 **Most significant protein abundance changes specific to planktonic and biofilm cells**

175 The Venn diagram in **Figure S2B** indicates the highest number of specifically identified
176 proteins on the SBFs (n , 173) and the lowest on the PBFs (n , 16), while no unique
177 identifications were detected for the PL cells. The uniquely detected proteins with the
178 highest raw intensity values included a signal transduction associated serine/threonine-

179 protein kinase (PknL), a LGFP-repeat protein specific to SBFs, and a β -1,3-endoglucanase
180 and bacterioferritin BfrA specific to PBFs (**Table S2**). The proteins detected with the
181 highest intensity values and only in the biofilm-ECMs included an error-prone polymerase
182 DinB, a preprotein sec-translocase subunit YajC, a cytochrome P-450 monooxygenase, a
183 PE family immunogen and a signal transduction-related adenylate cyclase involved in
184 cyclic di-AMP biosynthesis (**Table S2**).

185 Next, the log₂ transformed MaxLFQ data was subjected to pairwise comparisons to
186 indicate statistically significant protein abundance changes (**Table S3**). **Figure 3** shows
187 the greatest growth mode- and time-dependent fold-changes related for the PL vs. biofilms
188 cells, PBF vs. SBF cells and each biofilm subtype at different time points. Comparison of
189 the PL and both biofilm cells at their first timepoints of growth (PBF_2w and SBF_2d)
190 indicated the most prominent changes for PPE-family proteins (e.g., PPE61) and enzymes
191 involved in cell envelope biogenesis/metabolism (MurE, CwlM, cutinase and CelA1).
192 Among these, the PPE61 immunogen was ca. 6000- and 1800-times more abundant on
193 the PL compared to the PBF_2w and SBF_2d, respectively. CelA1, a β -1,4-
194 cellobiohydrolase known to prevent biofilm growth in *M. smegmatis* and Mtb (11, 18, 19),
195 was detected with 50- and 130-fold higher abundances on the PL compared to the PBFs
196 at the one-week and the SBFs at the two-day timepoints, respectively (**Table S3**).

197 Comparison of the PBF_2w and SBF_2d cells indicated Esx1-associated virulence factors
198 (i.e., EspF, EspA/EspE and ESAT-6) and PPE family immunogens as 30–130-fold more
199 abundant on the PBF than the SBF cells, meanwhile tricarboxylic acid (TCA)/glyoxylate
200 cycle-associated isocitrate lyase (ICL1) was over 200-fold more produced by the SBF than
201 the PBF cells. After 12 weeks, the proteins more abundant in the SBF compared to the
202 PBF included an LppP/LprE lipoprotein (ca. 16-fold), HemD involved in the synthesis of
203 vitamin B12 (ca.15-fold), FadD29 contributing to the synthesis of phenolic glycolipids (~13-

204 fold), β -lactamase able to hydrolase β -lactam antibiotics (ca. 9-times) and ICL1 catalyzing
205 the glyoxylate shunt-mediated activities (ca. 8-fold). More abundant proteins on the PBF at
206 this time-point were identified as a polysaccharide (N-acetylmuramic acid, MurNAc)
207 deacetylase PdaC (ca.15-fold) and a translocase subunit, SecE (ca.11-fold).
208 In the PBF, an MPB64 immunogen, siderophore export accessory protein MmpS5, several
209 Esx1-associated proteins (EspA/EspE, EspF) and adhesins (Ala-Pro-Ala rich protein APA
210 and fibronectin binding protein FAP) displayed the most significant abundance decreases
211 at the 12-week timepoint. In the SBFs, these proteins included a large-conductance
212 mechanosensitive channel protein Msc, a membrane protein acting as the cells' safety
213 valve to relieve osmotic pressure, arabinosyltransferases EmbA/EmbB, the Esx1
214 associated EspA/EspE and the MycP1 protease. Proteins with the greatest abundance
215 changes after 12 weeks in the SBFs included mammalian entry proteins (MCEs) and an α -
216 1,4-glucan:maltose-1-phosphate maltosyltransferase.

217

218 **Decreased CelA1 synthesis is also required for biofilm formation in *M. marinum***

219 As our findings suggest that a lack of CelA could also promote the biofilm formation in
220 Mmr, we tested this hypothesis by overexpressing the *celA1* gene in a Mmr strain
221 equipped with pTEC27 with the tdTomato fluorescent marker (29). First, the *celA1*
222 expression level in the transformed Mmr strain was confirmed by qPCR, indicating a ca.
223 150-times higher *celA1* transcription compared to the control strain carrying an empty
224 pTECV27 (**Fig. 4A**). Then we analyzed the morphology of both the SBFs and PBFs after
225 two weeks using the CelA1-strain with WDeM. As seen in **Figure 4B**, the CelA1-strain
226 showed altered morphology compared to the Mmr with pTEC27 (WT control strain). After
227 two weeks of growth the CelA1-strain SBF showed a less defined/loss of the lichen-like
228 morphology and lower total thickness when compared to the SBF control with pTEC27.

229 Similarly, the CelA1 overproduction in Mmr resulted in disrupted and fuzzy ribbon-like
230 cords associated with PBF-type biofilm growth, as the PBF cells with pTEC27 had well
231 defined and tight ribbon like structures.

232 CelA1 expression was recently linked with biofilm formation, antibiotic tolerance, and
233 virulence in Mtb (9). Therefore, Mmr cells in planktonic and biofilm forms with/without the
234 CelA1 overexpression were also exposed to rifampicin to determine the minimum
235 inhibitory (MIC) and minimum bactericidal concentration (MBC) for this bactericidal first-
236 line TB drug. **Figure 4C** shows that, in both the planktonic and biofilm cultures, CelA1
237 overexpression decreases the MIC/MBC, with a clear impact on two-day-old and 4-day-old
238 biofilms. These results indicate that CelA1 impedes biofilm formation and increases the
239 susceptibility of the residing cells to rifampicin in Mmr.

240

241 **Functional pathways specifically induced in planktonic and biofilm cells**

242 The LFQ proteomic data was next subjected to a PCA analysis for comparing growth
243 mode- and time-dependent protein abundance patterns on the PL cells and aging biofilms.
244 The PCA in **Figure 5A** shows clear clustering for each data set except for replicates
245 associated with two-week-old PBF-proteomes, which show greater variation. PC1,
246 separating the samples according to the growth mode, explains 39% of the total variation,
247 while 24% (PC2) of the variation can be explained by the age of the culture. The two-day-
248 old SBF-proteomes form a clearly distinguishable cluster, while the PL-proteomes and
249 proteomes associated with the PBFs between the two- and four-week time-points show
250 close clustering. Although the SBF- and PBF-proteomes differ greatly within the first four
251 weeks of growth, these biofilm subtypes seem to undergo similar proteome changes
252 during the later stages of growth, as proteomes of both subtypes clustered more closely at
253 the 12-week timepoint. Notably, PBFs during the first weeks (two to three weeks) of growth

254 shared a more similar ECM-proteome with the PL cells than the SBFs under the same
255 conditions.

256 Next, a multi-sample test (ANOVA) was conducted on the normalized LFQ intensity data to
257 investigate growth mode-dependent proteome differences at time points between two days
258 and three months. A dendrogram/ heatmap in **Figure 5B** shows hierarchically clustered
259 co-abundance data for 690 proteins having a statistically significant abundance change in
260 at least one of the conditions tested (**Table S4**). Six major clusters were clearly
261 distinguished, among which cluster 1 (n , 375) and cluster 6 (n , 125) contained the greatest
262 number of proteins, with higher abundances in one- to four-week-old SBFs (cluster 1) and
263 two-day- to two-week-old SBFs (cluster 6), respectively. STRING (Search Tool for the
264 Retrieval of Interacting Genes/Proteins) enrichment analyses performed on both clusters
265 (**Table S5**) indicated the greatest changes for pathways coordinating cell envelope
266 biogenesis/ metabolism, energy metabolism and protein secretion/export. **Figure 6A**
267 shows a protein-protein interaction (PPI) network for cluster 1 proteins: **(i)** cytoplasmic
268 proteins with a primary function in amino acid biosynthesis (*e.g.*, Gly, Asp, Tyr, Arg, His,
269 Thr, Ser, Lys, Phe), purine/pyrimidine metabolism (*e.g.*, PyrG, PurD/L/H, GuaB) and stress
270 response (HrcA, ClpC/X, DnaJ, HtpG, AhpC, SodC, RecA, Trx), **(ii)** proteins involved in
271 cell-wall/outer layer and mycomembrane biogenesis/metabolism (*e.g.*, PknA/B, Weg31,
272 CwsA, CwlM, PbpA1a, EmbA/B, KasA, DesA1/2, PpsA/B/D, PcaA, Fad enzymes), **(iii)**
273 components of the respiratory electron transport chain (SDH, FMR, Qcr-complex) and ATP
274 synthesis (F1F0 ATP synthase-complex), and **(vi)** proteins involved in iron
275 storage/homeostasis (ferritin). The PPI network analysis on the cluster 6 proteins indicated
276 the enrichment of metabolic activities related to translation (ribosomal proteins/r-proteins),
277 stress response (GroEL/ES, GrpE, DnaK, TF, ClpB) and the TCA/glyoxylate cycle (*e.g.*,
278 CitA, ICL1, FBA, GlcB) (**Fig. 6B**).

279 Clusters 2, 4 and 5 (n , 144) share co-abundance patterns, which indicate increased
280 protein abundances during the first weeks of growth in the PBFs when compared to the
281 SBFs. These contain virulence-, invasion- and viability/persistence-related proteins, such
282 as EsxA/B, ESX-EspB/G/M/P/N, Esx5-secretion associated protease MycP, cutinase
283 (Cut), a lysophospholipase (YtpA), endopeptidase (Lon), heparin binding hemagglutinin
284 (HbhA), fibronectin binding (Apa), catalase-peroxidase (KatG), and mammalian entry
285 proteins (MCEs). Cytoplasmic proteins were also detected in these clusters (e.g., ICL2,
286 ACN, ENO, GapDH, GPD, Tpi, PGK, MDH, ClpP1/2, CpsA/D, Trp, Cys, Met, an 18-kDa β -
287 CA) but their composition differs clearly from those in clusters 1 and 6. In addition, cluster
288 2 contains virulence-associated ESAT-6-like proteins, TDM-cord factor synthesis
289 associated Ag85A/C (mycolyltransferases), and an MPT64 immunogen with higher overall
290 abundancies on the PL and PBF cells compared to the SBFs. The remaining cluster 3 (n ,
291 47) differs from the other five by proteins with its overall higher abundancies on the PL
292 cells and/or on four- to 12-week-old PBFs when compared to the SBFs at the same
293 timepoints. One of these was identified as a potential trehalase (A0A2Z5YJK7_MYCMR),
294 a glycoside hydrolase that catalyzes the conversion of trehalose to glucose, which had a
295 high abundancy in four- and 12-week-old PBFs.

296 The protein identifications most relevant to biofilm growth and viability identifications are
297 listed in **Table S6** according to their predicted functions. The major growth mode-
298 dependent changes associate with the following five functional groups: **(i)** secretion
299 mechanisms, virulence, and adherence; **(ii)** cell wall/membrane/lipid biogenesis and
300 metabolism and biofilm formation; **(iii)** stress response; **(iv)** TCA/glyoxylate cycles and
301 carbohydrate metabolism; and **(v)** maintaining redox balance and energy metabolism. An
302 additional schematic model of the mycobacterial cell envelope in **Figure 7** illustrates the
303 key proteome changes relevant to the PL-, SBF- and PBF-type growth in Mmr.

304 **Time-kill curve analysis for indicating persister cells in maturing biofilms**

305 As growth mode-dependent differences imply higher persistence/tolerance-associated
306 activities in biofilms than in planktonic cultures, we next validated these findings by
307 exposing both the planktonic and biofilm cells to rifampicin and monitored cell death using
308 a time-kill curve analysis. This method enables the demonstration of an overall slower
309 killing efficacy for tolerant populations or a bimodal time-kill curve that indicates the
310 presence of a persistent bacterial subpopulation (31, 32).

311 First, we used a bacterial killing assay with bioluminescence as a readout to quantify the
312 tolerance/persistence in the planktonic cultures and two-week-old biofilms. The planktonic
313 and biofilm cells were treated with 400 $\mu\text{g mL}^{-1}$ rifampicin (64 x MIC, minimum inhibitory
314 concentration), and the rate of bacterial killing was monitored for seven days. The use of
315 bioluminescence as a readout for killing biofilm-associated bacteria was also assessed
316 using an OD₆₀₀-based method (**Fig. S3A**). The time-kill curve for the biofilm population
317 was bimodal, showing the faster killing of a susceptible subpopulation followed by a slower
318 killing of a persistent subpopulation of cells (**Fig. 8A**). These results indicate that Mmr
319 biofilms harbor significantly more persister cells than logarithmic phase planktonic
320 populations.

321 Next, the development of persistence in the biofilms was monitored by killing two-day-,
322 four-day-, and one-week-old biofilm cells with 64 x MIC rifampicin. Analysis of the time-kill
323 curves showed that persistence increases gradually in the maturing biofilms, reaching a
324 statistically significant increase in one-week-old biofilms compared to the planktonic cells
325 ($P = 0.0002$) (**Fig. 8B**). In untreated biofilms, the bioluminescence signal level continues to
326 increase well past the one-week timepoint, showing that the biofilm-associated
327 mycobacterial population is replicating and/or metabolically active at this stage (**Fig. S3B**).
328 This indicates that increased persistence is not (mainly) caused by the induction of

329 dormancy or metabolic inactivity. According to our experimental settings, PBFs form later
330 than SBFs and are visually detectable only after two weeks. Thus, this data shows that a
331 substantial persister subpopulation develops in SBFs by the first week of biofilm
332 development.

333 To test if the formation of persister cells differs between the two biofilm subtypes, PBFs
334 and SBFs were collected separately and tested with the time-kill assay under 64 x MIC
335 rifampicin. After seven days, the time-kill curves indicated no significant differences in the
336 rate of persistence between the two-week-old pellicle and submerged biofilms ($P = 0.51$)
337 (**Fig. 8C**). Thus, our results indicate that the proportion of persisters is greater in over one-
338 week-old Mmr biofilms than in logarithmic planktonic cell populations, and that the biofilm-
339 associated persistence increases over time.

340

341 **DISCUSSION**

342 **Mmr grows in morphologically distinct biofilm subtypes *in vitro***

343 A recent study confirmed that Mtb forms biofilm-like communities *in vivo*, which confers
344 increased tolerance to rifampicin and thus provides an explanation for the chronic nature
345 of TB (11). The present study shows that Mmr grows in two different biofilm subtypes, and
346 that reduced CelA1 hydrolase activity is one of the main triggers of biofilm growth and
347 increased tolerance to rifampicin in both biofilm subtypes. Studies on Mtb and *M.*
348 *smegmatis* have demonstrated that cellulose filaments are vital structural constituents of
349 mycobacterial biofilm-ECMs as well as essential for biofilm formation and the development
350 of tolerance/persistence (9, 11, 18, 19). We also show that the Mmr biofilm subtypes show
351 distinct morphologies, with SBFs containing lichen-like structures and PBFs consisting of
352 ribbon-like cords under the same *in vitro* conditions. Biofilm growth accompanied by
353 cording-like growth morphology is also reported for other mycobacteria and Mtb, in which

354 the surface interactions mediated by e.g., mycolic acids modulating the
355 mycomembrane/capsule hydrophobicity (11, 33). The proteomic data presented here
356 suggest that subtype-specific changes in cord-factor TDM-synthesis (mycolyltransferase
357 Ag85), Esx1-secretion, phthiocerol dimycocerosate (PDIM) export (MmpL7), MA
358 cyclopropanation (PcaA/Cma2), and lectin synthesis (33-37) may have affected the
359 mycomembrane composition and thereby contributed to distinct biofilm growth
360 morphologies in Mmr.

361

362 **Mmr may use membrane vesicles to deliver proteins in the biofilm-ECM**

363 The LFQ proteomics identified cytoplasmic proteins and proteins associated with the inner-
364 /mycomembrane as the largest protein group in both the planktonic and biofilm cells.
365 These findings are supported by studies identifying cytoplasmic proteins in the capsule of
366 another Mmr strain (E11) and by showing that their number increases when mycobacterial
367 cells grow in the biofilms, as demonstrated for *M. bovis* (17, 20). Membrane vesiculation is
368 the most likely explanation for their presence on Mmr cells and within the biofilm-ECM, as
369 several reports have demonstrated the presence of MVs on mycobacterial cells (38) as
370 well as trapped in biofilm-ECMs in other bacteria (39). In addition, several of the
371 cytoplasmic and inner-/mycomembrane-proteins detected here, including e.g., enzymes
372 involved in cell wall synthesis and lipid/ fatty acid metabolism, were previously identified in
373 MVs released by *Mycobacterium avium* 104 in response to starvation (40). Mycobacteria
374 have been shown to form MVs from mycomembrane (mMV) during normal growth (cell
375 lysis/death) and/or from inner-membrane (iMV) by blebbing in response to stress (e.g.,
376 iron-limitation and anoxia) (38). This report supports the idea that the identified myco-
377 /inner-membrane-proteins could have also entered the biofilm-ECMs by MVs in our study.
378 We further propose that CwIM, a N-acetylmuramoyl-L-alanine amidase (41, 42), detected

379 in one-week-old SBFs, is involved in this process, as weakening the link between the
380 mycomembrane and peptidoglycan has been suggested to stimulate MV blebbing in the
381 mycobacteria (38). Taken together, these findings may explain why more cytoplasmic
382 proteins were detected on this biofilm subtype, as the maturing biofilm cells grow under
383 reduced oxygen tension and anoxia is one of the factors able to trigger the membrane
384 vesiculation.

385 Bacterial MVs are involved in i.e., cell-cell communication, biofilm formation, virulence,
386 antibiotic resistance, iron scavenging, nutrient acquisition and modulating the host immune
387 system (43). We detected several cytoplasmic proteins involved in signal transduction
388 (e.g., PknL specific to SBFs and an adenylate cyclase detected only in biofilm-ECMs) and
389 enzymes involved in biofilm formation. GroEL1 and Fatty-Acid-Synthase system (FAS-I
390 and FAS-II) enzymes were among the detected proteins that coordinate biofilm formation
391 in mycobacteria. The GroEL1 chaperone is involved in the synthesis of mycolic acids
392 (MAs) that eventually become inserted in the mycomembrane as trehalose dimycolates
393 (TDM) and monomycolates (TMM) beneath the capsule (14, 21). This chaperone interacts
394 with ketoacyl-ACP synthase KasA (FAS-II) to modulate the synthesis of short-chain MAs
395 specifically during biofilm formation (21). A lack of GroEL1 has been reported to prevent
396 the biofilm formation and to affect the biosynthesis and composition of MAs in
397 *Mycobacterium bovis* BCG, whereas the GroEL1 deficiency blocks the formation of mature
398 biofilms in *M. smegmatis* (21, 24). In addition, the overexpression of KasA and the
399 inactivation of other FAS-II enzymes, such as enoyl-ACP reductase (InhA) and 3-oxoacyl-
400 [acyl-carrier-protein] synthase 2 (KasB), have also been reported to prevent biofilm
401 formation and formation of cords by reducing the cyclopropanation of MAs (14, 21, 25).
402 Here, GroEL1, KasA and InhA were detected as more abundant in the SBFs, implying that

403 these enzymes could support the initial stages of SBF-type biofilm growth, as GroEL and
404 KasA were detected with the highest abundancies already on the two-day-old SBFs.
405 Although no cell lysis was seen during the sample preparation for proteomic analysis
406 **(Table S7)**, we cannot exclude the possibility that some of the cytoplasmic or inner-/myco-
407 membrane-proteins were released by autolysis during growth. In other Gram-positive
408 bacteria, cytoplasmic proteins reach the extracellular space via regulated autolysis
409 (involving autolysins/peptidoglycan hydrolases), and, as soon as the pH of the culture
410 medium drops (due to the active metabolism of the growing cells), many of the released
411 proteins show an enhanced ability to bind to the cell wall and biofilm-ECM structures (43-
412 48). SBF cells are exposed to hypoxic conditions, and oxygen limitation acidifies the
413 biofilm matrix (48), allowing for a more efficient interaction between the cytoplasmic
414 proteins and biofilm-ECM structures. Thus, this could explain the presence of r-proteins as
415 the largest cytoplasmic protein group already on two-day-old SBFs; the strong positive
416 charge of these proteins has been proposed to mediate electrostatic interactions with
417 anionic cell-surface components, which promotes cell aggregation and biofilm stabilization
418 (48). Since the exposed mycomembranes with MAs as the major components create a
419 condition stimulating an interaction with many cytoplasmic proteins, pH-dependent binding
420 with the cell surface components could also explain why cytoplasmic proteins were
421 detected on Mmr cells grown on Tween-80.

422

423 **Biofilm subtypes differ in terms of secreted virulence and adhesion factors**

424 The proteomics data indicated that the mycomembrane-associated PPE/PE family
425 proteins were remarkably greater in number in the PL than in the PBFs or SBFs, indicating
426 that Mmr in a single cell state could more readily interact with the host, and modulate the
427 host immune response and/or nutrient transport (49, 50). PL cells were cultured in the

428 presence of Tween-80, which, in detaching the mycobacterial capsule (17), most likely
429 helped identify these immunogens. Tween-80 can also induce alterations in the
430 morphology, pathogenicity, and virulence of mycobacteria (51). For example, genes
431 encoding lipases and cutinases have been shown to be significantly upregulated in Mtb in
432 response to this nonionic surfactant. Our data is in line with this by showing that several
433 lipases/cutinases, with a likely ability to hydrolyze Tween-80, were more abundant on PL
434 cells compared to biofilms. As Tween-80 is considered to mimic a lipid rich milieu of
435 macrophages (51), the detected PL-proteome changes here may reflect a metabolic
436 adaption to conditions faced in vivo.

437 Our findings also suggest that Mmr uses different T7SS pathways in SBFs and PBFs for
438 virulence and adherence. For example, the Esx1-secretion components and substrates
439 (EsxA/B, EspB, EspF, EccA1, EspG1, EspH, EspL and MycP) were detected as more
440 abundant in the PBFs, while those associated with the Esx5-type secretion were overall
441 more abundant in the SBFs (Ecc, EspG, PPE/PE proteins). Both secretion pathways can
442 contribute to virulence and subverting the host immune system in Mtb (52). The major
443 subtype-dependent differences between the PBFs and SBFs were related to invasion and
444 adherence, including the MCE proteins, fibronectin binding APA and HphA, which can
445 modulate host cell signaling as well as aid adhesion or entry into host cells (53-55). All
446 these proteins were significantly more produced on the PBFs than the SBFs, and, in the
447 case of MCEs, may also involve MVs, as these adhesins are located on the inner
448 membrane of the mycobacterial cell wall. HphA also has implications in promoting cell-cell
449 aggregation in Mtb (56), suggesting that this adhesin could also contribute to cording
450 during PBF-type growth.

451

452

453 **Biofilm subtypes use different tolerance- and persistence-conferring mechanisms**

454 Tolerance is defined as the extent of time that bacteria can survive in the presence of a
455 high antibiotic concentration (31), whereas persisters are a subpopulation of
456 phenotypically drug tolerant cells that do not grow in the presence of an antibiotic (32). We
457 show that antibiotic killing of biofilm cells occurs at a significantly slower rate when
458 compared to PL cells. The time-kill curve indicated the temporally increased formation
459 of a persistent subpopulation with slower killing kinetics as well as the formation of
460 persisters in SBFs already after one week. At this stage, Mmr biofilms remained
461 metabolically active and replicating, indicating that persistence develops due to phenotypic
462 differentiation during biofilm growth rather than via the induction of dormancy.

463 The proteomic findings suggest that Mmr could use both overlapping and subtype-specific
464 mechanisms for increasing its tolerance and persistence, in which MVs or other non-
465 classical routes for protein export may play a role. Here, most significant proteome
466 changes related to cytoplasmic and inner-/mycomembrane-proteins and included
467 enzymes/proteins involved in the TCA cycle and glyoxylate shunt, mycolic acid synthesis
468 stress response, and energy and redox metabolisms. A recent transcriptome analysis of
469 another non-tuberculous mycobacterial model, *Mycobacterium abscessus*, supports our
470 findings; biofilm growth activated the glyoxylate shunt, redox metabolism and the MA
471 synthesis-associated elongation and desaturation pathways. The TCA cycle associated
472 enzyme CitA was recently reported to control the asymmetric cell division in *Caulobacter*
473 *crescentus* (57). This process has been shown to lead to the formation of heterogenous
474 cell populations in biofilms, macrophages, and granulomatous lesions also in mycobacteria
475 (7, 58, 59). Here, our findings indicated the presence of this enzyme on one-week-old
476 SBFs, suggesting that the asymmetric cell division occurs before the PBFs are formed.
477 Moreover, arabinosyltransferases EmbA and EmbB, involved in the polymerization of the

478 arabinogalactan, were also detected with high abundances in SBFs by one week onward,
479 suggesting that strengthening the arabinogalactan could further help residing cells,
480 including the persisters, increase their tolerance to rifampicin, as demonstrated with Mtb
481 persisters under hypoxia (60). Taken together, these findings strengthen the hypothesis
482 that persisters are indeed formed in one-week-old SBFs, and supports the results obtained
483 with the biofilm killing assay on the SBFs at this time point.

484 We also suggest that cells in PBFs use different TCA cycle enzymes, such as aconitase
485 (ACN), malate dehydrogenase (MDH), enolase (ENO), and/or fructose-bisphosphate
486 aldolase (FBA), to maintain long-term survival. In other gram-positive bacteria these
487 enzymes belong to known moonlighting proteins with established secondary roles outside
488 of the bacterial cell (e.g., adhesion)(30). In mycobacteria, these enzymes have been
489 reported to contribute to increased viability or persistence (61-63). The associated
490 glyoxylate shunt could also be involved (64), as isocitrate lyase 1 (ICL1) was detected as
491 more abundant on the SBFs, implying that this enzyme could help residing cells increase
492 their antioxidant defense and antibiotic tolerance (65). In contrast, ICL2 was produced
493 more on the PBFs, which may help the cells to survive under starvation conditions when
494 fatty acids are used as the primary carbon source (66). This is in line with the temporally
495 increased production of diacylglycerol O-acyltransferase (Tgs1) in PBFs, which can
496 promote the accumulation of triacylglycerols (TAGs); a process that has been considered
497 a hallmark feature of persisting Mtb/latent TB and a long-term energy source for Mtb and
498 have been found in substantial amounts in the mycobacterial cell wall (67, 68). The
499 detection of trehalase as significantly more abundant in four- to 12-week-old PBFs,
500 strengthens the idea that cells within this biofilm subtype suffer from nutrient stress and
501 activate trehalose salvage/recycling to promote redox and energy homeostasis, as seen
502 under carbon limitations in Mtb (69). These findings may also explain the detection of

503 proteases, chaperones, and assisting stress-proteins in high numbers in the biofilm-ECMs,
504 including e.g., the proteases Clp/Lon and the cold-shock protein CpsD, with known
505 implications in stringent response, persistence and/or post-antibiotic recovery (70-72).
506 These proteins were detected here as more abundant in the PBFs than in the SBFs,
507 implying that these pathways are preferred in PBFs to maintain viability.

508 A recent study comparing high numbers of persister Mtb mutants using genomics and
509 transcriptomics indicated a significant upregulation of energy production pathways and
510 pathways involved in redox reactions (oxidoreductase) (73). The ECM-proteome changes
511 occurring during SBF-type growth are in line with this report, as the components of the
512 respiratory electron transfer chain (cytochrome bc₁ complex, cytochrome c terminal
513 oxidase, and F₀F₁-ATPase synthase) were detected as more abundant on the SBFs
514 facing more hypoxic conditions than the PBFs. Our findings also agree with previous
515 reports showing that the electron transfer chain is essential for maintaining ATP
516 homeostasis and the viability of nonreplicating/persistent Mtb cells under hypoxia (74-76).
517 In addition, we show that both redox and iron metabolism could also play a biofilm
518 subtype-specific role in helping the cells cope with hypoxia/aeration-related stress (77);
519 several oxidoreductases, thioredoxin and a superoxide dismutase (SOD) were overall
520 more abundant in the SBFs, and a catalase-peroxidase (KatG) and alkyl
521 hydroxyperoxidases (AhpCF) as more abundant in the PBFs. These enzymes have been
522 shown to protect Mtb against oxidative stress by the reduction of superoxide radicals into
523 less toxic intermediates for inhibiting autophagy, apoptosis and cellular damage (78). Iron
524 storing proteins ferritin (BfrB) and bacterioferritin (BfrA) can confer increased redox
525 resistance on Mtb and protect the cells against oxidative stress and hypoxia, respectively
526 (79). Here, these iron storing proteins displayed biofilm subtype-specific abundance

527 changes, implying that SBFs could rely on BfrB to cope with hypoxia and PBFs on BrfA to
528 help cells grow at the air–liquid interface.

529

530 **CONCLUSIONS**

531 The present study reports an in-depth view of ECM-proteome changes occurring in Mmr
532 ATCC927 during biofilm growth in vitro from two days to three months. We show that this
533 non-tuberculous mycobacterial model forms SBFs already after two days, whereas the
534 formation of detectable PBFs was observed after two weeks of growth in the absence of
535 Tween-80. Both biofilm subtypes were formed physically under the same conditions with
536 clearly distinct growth morphologies: SBFs with lichen-like structures and PBFs with
537 ribbon-like cords. We show that the reduced CelA1-mediated cellulose hydrolysis is
538 necessary to establish proper biofilm growth, growth morphology and increased tolerance
539 to rifampicin for both biofilm subtypes. The formation of persisters in both biofilm subtypes
540 and increased tolerance was further confirmed by the newly established bioluminescence-
541 based time-kill assay, which provides an effective tool for quantifying tolerance and
542 persistence in Mmr. The proteomic findings imply that subtype-dependent changes in the
543 MA synthesis and modification, Esx1-type secretion, and the production of specific
544 adhesins were the major drivers of distinct biofilm growth morphologies. We also propose
545 that pathways associated with MA biosynthesis, development of tolerance/persistence and
546 oxidative/redox stress are differentially used in PBFs and SBFs to maintain prolonged
547 viability. Possible explanations for these differences include the different oxygen tensions
548 encountered by the biofilm subtypes, differences in membrane vesiculation activities
549 and/or other non-classical pathways for protein export. Taken together, this is the first
550 study reporting on ECM-proteome dynamics in maturing mycobacterial biofilms and
551 predicting biofilm subtype-specific changes in cell-cell communication, biofilm matrix

552 formation, virulence, and tolerance/persistence. This is also the first time that the kinetics
553 of persistence have been explicitly measured from mycobacterial biofilms.

554

555 **MATERIALS AND METHODS**

556 **Preparing bacterial cells for surface proteomics**

557 *Mycobacterium marinum* (ATCC 927) with the pTEC27 plasmid expressing the red
558 fluorescent protein tdTomato (Addgene #30182, <http://n2t.net/addgene:30182>) (29) was
559 pre-cultured on Middlebrook 7H10 plates with 10% (v/v) Oleic Albumin Dextrose Catalase
560 (OADC) enrichment (Fisher Scientific, NH, USA) and 0.5% (v/v) glycerol at 29 °C for one
561 week. For planktonic cultures, an inoculum of Mmr was transferred into a Middlebrook 7H9
562 medium supplemented with 10% (v/v) ADC (Fisher Scientific, NH, USA), 0.2% (v/v)
563 glycerol, and 0.2% (v/v) Tween-80 (Sigma-Aldrich, MO, USA), and the cells were cultured
564 at 29 °C in cell culture flasks with filter caps. After three days of incubation the cell cultures
565 were diluted to obtain an OD₆₀₀ of 0.042 and the dilutions were cultured for an additional
566 2 days at +29 °C until harvesting. For the biofilm cultures, a Middlebrook 7H9 medium with
567 the ADC growth supplement but without Tween-80 or glycerol was used. The inoculum
568 was cultured for three days at +29 °C until the OD₆₀₀ reached 0.45. The cell cultures were
569 diluted 1:40, and the dilutions were divided into 10 ml aliquots. The cap of each tube was
570 sealed with Parafilm M® laboratory wrapping film, and the cultures were incubated at +29
571 °C. Planktonic and biofilm cell samples (SBFs and PBFs separately) were collected at the
572 time points indicated in **Figure 2A**. All the cultures were performed in quadruplicates.
573 Planktonic cells were harvested by centrifugation (3 min, 5 000g, +4 °C) and the pelleted
574 cells were suspended gently in ice-cold buffer (100 mM Bis-Tris, pH 6.5) to remove
575 interfering/non-specifically bound proteins. This step prevents the detachment/removal of
576 cytoplasmic moonlighters bound to the cell surfaces/biofilm-ECM (43-46, 79, 80). The

577 PBFs were collected with an inoculation loop, the extra medium was removed by pipetting
578 to avoid cross-biofilm type contamination, and the SBFs were harvested by
579 pipetting/scraping. The PBFs and SBFs were collected in separate Eppendorf tubes the
580 ice-cold buffer (100 mM Bis-Tris, pH 6.5). Cells (planktonic and biofilm cultures) were
581 pelleted by centrifugation (3 min, 5 000g, +4 °C) and the washed cells were suspended
582 gently in 95 µL of 100 mM TEAB (triethylammonium bicarbonate, pH 8.5) for the enzymatic
583 shaving reaction.

584

585 **Trypsin/Lys-C shaving of planktonic and biofilm cells**

586 Peptides from cell-surface/biofilm-ECM-associated proteins were released via a
587 Trypsin/Lys-C mix (Promega) at a final concentration of 50 ng µL⁻¹, and the digestions
588 were incubated at 37 °C for 20 minutes. The method was validated by counting the
589 number of colonies formed on the planktonic/single and biofilm cells treated with/without
590 the enzyme mix (**Table S7**). The released peptides and the enzymes were recovered by
591 filtration through a 0.2 µm acetate membrane (Costar® Spin-X Centrifuge Tube Filter,
592 Corning Inc., Corning, NY, US) by centrifugation (8000g, 3 min, 20 °C). Flow-troughs were
593 incubated for 16 hours at 37 °C. The concentration of released peptides in each sample
594 was measured with a NanoDrop2000 spectrophotometer (Thermo Scientific). Digestions
595 were terminated with 0.6% (v/v) trifluoroacetic acid (TFA) (Sigma Aldrich) and the peptides
596 were purified using ZipTip C18 (Millipore) according to the manufacturer's instructions and
597 dried using a miVac centrifugal vacuum concentrator (GeneVac).

598

599 **LC-MS/MS analysis**

600 The peptides were dissolved in 0.1% (v/v) formic acid (FA) and analyzed with nanoLC-
601 MS/MS using an Easy-nLC 1000 nano-LC system (Thermo Scientific) coupled with a

602 quadrupole Orbitrap mass spectrometer (Q ExactiveTM, ThermoElectron, Bremen,
603 Germany) as previously reported (80). The obtained MS raw data was processed via
604 MaxQuant software (version v.1.6.1.0) with the built-in search engine, Andromeda (81,
605 82), using a protein database comprising all 5,564 Mmr protein sequences (Uniprot
606 proteome: up000257451, genome accession: PEDF01000000) both forward and reverse.
607 Carbamidomethyl (C) was set as a fixed and methionine oxidation was set as a variable
608 modification. Tolerance was set to 20 ppm in the first search and 4.5 ppm in the main
609 search. Trypsin without the proline restriction enzyme option and with two allowed
610 miscleavages was used. The minimal unique plus+ razor peptide number was set to 1; the
611 FDR was set to 0.01 (1%) for peptide and protein identification; and LFQ with default
612 settings was used. The mass spectrometry proteomics was deposited in the
613 ProteomeXchange Consortium via the PRIDE (83) partner repository with the dataset
614 identifier PXD02010.

615

616 **Proteome statistics and bioinformatics**

617 The identified Mmr proteins were manually curated by characterizing hypothetical and
618 tentatively annotated proteins with the aid of the Basic Local Alignment Search Tool
619 (BLAST) program from the National Center for Biotechnology Information (NCBI) (84-86),
620 combined with CDD/SPARCLE conserved domain identification (87) and SmartBLAST
621 (UniProt) searches. General protein functions were annotated using the Gene Ontology
622 (GO) database (88). Isoelectric points (pIs) and molecular weights (MWs) for the identified
623 proteins were predicted using EMBOSS Pepstats (89) at [https://www.ebi.ac.](https://www.ebi.ac.uk/Tools/seqstats/emboss_pepstats/)
624 [uk/Tools/seqstats/emboss_pepstats/](https://www.ebi.ac.uk/Tools/seqstats/emboss_pepstats/). The presence of possible protein secretion motifs
625 (classical and nonclassical) for all the predicted and identified proteins was obtained with
626 SignalP4.1 (90) (<http://www.cbs.dtu.dk/services/SignalP/>) and SecretomeP 2.0/SecP (91)

627 (<http://www.cbs.dtu.dk/services/SecretomeP/>). The presence of transmembrane spanning
628 domains/helices (TMDs) was determined with the TMHMM Server v. 2.0 at <http://www.cbs.dtu.dk/services/TMHMM/> (92, 93) for the identified proteins.
629
630 For indicating statistically significant abundance changes the log₂-transformed LFQ data
631 was analyzed in Perseus v.1.6.2.3 (94) using a Student's *t*-test with permutation-based
632 FDR adjustment. For the multivariate analyses, the missing values were replaced by
633 imputed values from the normal distribution (width = 0.3, down shift = 1.8) and then
634 normalized (z-score) prior to ANOVA for multi-sample testing (S0 set to 0.1 and a
635 permutation-based FDR of 5%) and hierarchical clustering/PCA. STRING Protein
636 Interaction Network and Functional Enrichment Analyses (GO, KEGG, InterPro, Pham)
637 were studied using the STRING database v. 11 (95). Interaction scores were set to high
638 (0.700) confidence, and the interacting proteins were clustered using Markov clustering
639 (MCL) with the inflation parameter set to 4.0–6.0. Functional enrichments were statistically
640 assessed with both rank- and gene set-based approaches (FDR of 0.05).

641

642 **Creation of the CelA1 overexpression construct in Mmr**

643 The Mmr CelA1 overexpression strain was created by ordering the MMAR_0107 open
644 reading frame in the pUC57 vector with appropriate restriction sites from GenScript and
645 subcloning the construct into the pTEC27 vector (AddGene) (29), which carries the red
646 fluorescent protein tdTomato. The sequence of the plasmid was confirmed by sequencing.
647 The resulting plasmid was transformed into an electrocompetent Mmr ATCC927 strain.
648 Transformants were selected on Middlebrook 7H10 agar plates containing 10% (v/v)
649 OADC enrichment, 0.5% (v/v) glycerol and 75 µg mL⁻¹ hygromycin.

650

651

652 **RNA and DNA extractions**

653 For RNA and DNA extractions, the *CelA1* overexpression strain and Mmr were precultured
654 on MiddleBrook 7H10 plates and transferred into the Middlebrook 7H9 medium described
655 above (75 $\mu\text{g mL}^{-1}$ hygromycin for the *CelA1* strain). After three days, the bacterial cells
656 were harvested, pelleted, and homogenized in TRI Reagent (Thermo Fisher Scientific, NH,
657 USA) with ceramic beads using the PowerLyzer24 (Mobio, CA, USA). After
658 homogenization, the samples were sonicated for nine minutes and the RNA and DNA
659 were extracted according to the manufacturer's instructions.

660

661 ***CelA1* expression and the quantification of mycobacterial loads by qPCR**

662 Prior to qPCR analysis, RNA was reverse transcribed into cDNA with a Reverse
663 Transcription kit (Fluidigm, CA, USA) according to the manufacturer's instructions. *CelA1*
664 expression was measured using soFast EvaGreen Supermix with the Low ROX qPCR kit
665 (Bio-Rad, CA, USA) and the CFX96 qPCR system (Bio-Rad, CA, USA). The primers used
666 for *CelA1* were: (forward: 5'- ACACTCCGCAGTCCTACT-3' and reverse: 5'- TAGAGCGTC
667 AGAATCGGC-3'). The number of mycobacterial cells in the sample was quantified using
668 the SensiFAST SYBR No-ROX qPCR kit (Bioline, London, UK) on bacterial DNA
669 according to the manufacturer's instructions. The primers used for Mmr quantification were
670 targeted against 16S-23S, locus AB548718 (forward: 5'- CACCACGAGAAACTCCAA-3'
671 and reverse: 5'- CACCACGAGAAACTCCAA-3'). Each bacterial quantification qPCR
672 run included a standard curve of the known amounts of Mmr DNA. The mycobacterial cell
673 number in each sample was used to normalize the *CelA1* expression.

674

675

676

677 **Widefield deconvolution microscopy (WDeM) of Mmr biofilms**

678 PBFs and SBFs formed by Mmr with pTEC27 (WT), expressing the red fluorescent protein
679 tdTomato (29), and Mmr overexpressing *CelA1* were prepared as follows. Briefly, the cells
680 were incubated at 29 °C and the surface-attached cells were imaged at seven, 14 and 21
681 days after dilution. In situ imaging of the SBFs was conducted with Nikon FN1 upright
682 epifluorescence microscope equipped with 20x/0.8 dry objective, Hamamatsu ORCA-
683 Flash4.0 V3 Digital CMOS camera and CoolLED pE-4000 light source. tdTomato was
684 excited with 550 nm LED and fluorescence was collected with 617/73 band-pass emission
685 filter. Image stack were collected with 2µm intervals (x-y pixel size 325 nm). The data was
686 deconvolved with Huygens Essential deconvolution software (SVI, Amsterdam,
687 Netherlands) using 200 iteration limit, signal-to-noise ratio of 30 and quality threshold of
688 0.01.

689

690 **Biofilm tolerance assays**

691 The role of *CelA1* overexpression in the antibiotic tolerance of Mmr was assessed as
692 follows. First, the *CelA1* overexpression strain and pTEC27 control strain were cultured
693 for one week on 7H10 plates (10% OADC, 0.5% glycerol + 75 µg mL⁻¹ hygromycin) and
694 then transferred in a Middlebrook 7H9 medium supplemented with 10% ADC and 75 µg
695 mL⁻¹ hygromycin) at an OD₆₀₀ of 0.1 to initiate biofilm growth. Aliquots of bacterial
696 suspension (192 µl of per well) were added to 96-well-plates in triplicate, sealed with
697 parafilm and incubated at +29 °C in the dark. Planktonic cultures grown in the presence of
698 0.2% glycerol were used as controls. Eight µl of antibiotics per well was added two, four,
699 seven and 14 days after the start of the liquid culture. The final antibiotic concentrations
700 used were 400, 100, 25 and 6.25 µg mL⁻¹ for the Rifampicin TOKU-E solution. Untreated
701 wells were used as controls. Ten µl per sample was plated on 7H9 plates (10% OADC, 75

702 $\mu\text{g mL}^{-1}$ hygromycin) one week after the addition of antibiotics. The plates were incubated
703 at +29 °C for seven to nine days and the colonies were counted.

704

705 **Biofilm persistence assays**

706 Mmr (ATCC 927) with a bioluminescence cassette in the pMV306hsp+LuxG13 plasmid
707 was used for antibiotic tolerance assays. pMV306hsp+LuxG13 was provided by Brian
708 Robertson and Siouxsie Wiles (Addgene plasmid #26161; [http://n2t.net/addgene: 26161](http://n2t.net/addgene:26161)).
709 To measure the kinetics of bacterial killing, the bioluminescent Mmr strain was first
710 cultured on Middlebrook 7H10 agar (Sigma-Aldrich) supplemented with 0.5% (v/v) glycerol
711 (Sigma-Aldrich) and 10% (v/v) OADC enrichment (BD, Becton Dickinson) at 29 °C for
712 seven days in the dark. To initiate biofilm formation, the Mmr cells were suspended in
713 Middlebrook 7H9 broth (Sigma-Aldrich) supplemented with 10% (v/v) ADC enrichment
714 (BD, Becton Dickinson) at a starting OD_{600} of 0.1. Planktonic cultures were prepared in the
715 same way except that the medium contained 0.2% (v/v) glycerol (Sigma-Aldrich) and 0.2%
716 (v/v) Tween-80 (Sigma-Aldrich). Bacterial suspensions (192 μL per well in triplicates) were
717 divided on to white 96-well plates (Perkin Elmer). The biofilm cultures were sealed with
718 laboratory film and incubated at 29 °C in the dark to the desired ages. Rifampicin solution
719 (TOKU-E) in water at a final concentration of 400 $\mu\text{g mL}^{-1}$ corresponding to 64 x MIC
720 (minimum inhibitory concentration) was added to the bacterial suspensions and incubated
721 for seven days at 29 °C in the dark. The bioluminescence signal was measured with an
722 EnVision plate reader (Perkin Elmer) as a readout for bacterial survival three times for
723 three seconds per well daily from a white 96-well plate for seven days. The background
724 signal from media only wells was first subtracted from the sample wells and an average of
725 the three measurements normalized with the starting bioluminescence signal was used to

726 draw time-kill curves of the bacterial population in the biofilms at different maturation
727 stages.

728 To compare the level of persistence/tolerance in the PBFs and SBFs, Mmr was cultured in
729 a total volume of 10ml at the starting OD₆₀₀ value of 0.1. After two weeks, the biofilms were
730 collected separately from the tubes by lifting the pellicle with a 1- μ L inoculation loop
731 coupled with careful pipetting. The pellicle and submerged biofilms were centrifuged at
732 10,000g for three minutes, the supernatants were collected, and the wet weight of the
733 bacterial mass was measured. The bacterial cells were suspended into previously
734 collected spent media at the concentration of 15 mg mL⁻¹, vortexed briefly, and divided on
735 white 96-well plates (Perkin Elmer) with 192 μ L of cell suspension per well in triplicate.
736 Eight μ L of TOKU-E solution at a final concentration of 400 μ g mL⁻¹ were pipetted on the
737 bacterial suspension. Liquid cultures were incubated for seven days at 29 °C in the dark
738 and the bioluminescence signal was measured daily with an EnVision plate reader (Perkin
739 Elmer) three times for three seconds per well. The background signal from the media-only
740 wells was first subtracted from the sample wells, and an average of the three
741 measurements was normalized with the starting bioluminescence signal measured just
742 before adding the rifampicin. The statistical significance of the differences between the
743 time-kill curves was tested with a log-rank test using Prism5 software (GraphPad).

744

745 **ACKNOWLEDGEMENTS**

746 The financial support of the Academy of Finland (projects no. 322010 (AF, JYK, MP) and
747 326674 (MP), Jane and Aatos Erkko Foundation (MP), Sigrid Jusélius Foundation (MP),
748 Foundation of the Finnish Anti-Tuberculosis Association (Suomen Tuberkuloosin
749 Vastustamisyhdistyksen Säätiö)(HL, LMV, KS) and Tampere Tuberculosis Foundation
750 (MP, KS, HM, HL, LMV) is greatly appreciated. Mass spectrometry-based proteomic

751 analyses were performed by the Proteomics Core Facility, Department of Immunology,
752 University of Oslo/Oslo University Hospital, which is supported by the Core Facilities
753 program of the South-Eastern Norway Regional Health Authority. This core facility is also a
754 member of the National Network of Advanced Proteomics Infrastructure (NAPI), which is
755 funded by the Research Council of Norway INFRASTRUKTUR-program (project number:
756 295910)(TAN).

757

758 REFERENCES

759

- 760 1. Global tuberculosis report 2020. Geneva: World Health Organization; 2020. Licence:
761 CC BY-NC-SA 3.0 IGO.
- 762 2. Panjabi R, Comstock GW, Golub JE. 2007. Recurrent tuberculosis and its risk
763 factors: adequately treated patients are still at high risk. *Int J Tuberc Lung D* 11:828-
764 837.
- 765 3. Rosser A, Marx FM, Pareek M. 2018. Recurrent tuberculosis in the pre-elimination
766 era. *Int J Tuberc Lung D* 22:139-150.
- 767 4. Aldridge BB, Fernandez-Suarez M, Heller D, Ambravaneswaran V, Irimia D, Toner
768 M, Fortune SM. 2012. Asymmetry and aging of mycobacterial cells lead to variable
769 growth and antibiotic susceptibility. *Science* 335:100-104.
- 770 5. Malherbe ST, Shenai S, Ronacher K, Loxton AG, Dolganov G, Kriel M, Van T, Chen
771 RY, Warwick J, Via LE, Song T, Lee M, Schoolnik G, Tromp G, Alland D, Barry CE,
772 3rd, Winter J, Walzl G, Catalysis TBBC, Lucas L, Spuy GV, Stanley K, Thiart L, Smith
773 B, Du Plessis N, Beltran CG, Maasdorp E, Ellmann A, Choi H, Joh J, Dodd LE,
774 Allwood B, Koegelenberg C, Vorster M, Griffith-Richards S. 2016. Persisting positron
775 emission tomography lesion activity and *Mycobacterium tuberculosis* mRNA after
776 tuberculosis cure. *Nat Med* 22:1094-1100.

- 777 **6.** Jankute M, Cox JA, Harrison J, Besra GS. 2015. Assembly of the Mycobacterial cell
778 wall. *Annu Rev Microbiol* 69:405-423.
- 779 **7.** Sarathy JP, Via LE, Weiner D, Blanc L, Boshoff H, Eugenin EA, Barry CE, 3rd,
780 Dartois VA. 2018. Extreme drug tolerance of *Mycobacterium tuberculosis* in caseum.
781 *Antimicrob Agents Chemother* 62:e02266-17.
- 782 **8.** Basaraba RJ, Ojha AK. 2017. Mycobacterial biofilms: Revisiting tuberculosis bacilli in
783 extracellular necrotizing lesions. *Microbiol Spectr* 5:10.1128/microbiolspec.TBTB2-
784 0024-2016.
- 785 **9.** Chakraborty P, Bajeli S, Kaushal D, Radotra BD, Kumar A. 2021. Biofilm formation in
786 the lung contributes to virulence and drug tolerance of *Mycobacterium tuberculosis*.
787 *Nat Commun* 12:1606.
- 788 **10.** Handwerger S, Tomasz A. 1985. Antibiotic tolerance among clinical isolates of
789 bacteria. *Annu Rev Pharmacol Toxicol* 25:349-380.
- 790 **11.** Chakraborty P, Kumar A. 2019. The extracellular matrix of mycobacterial biofilms:
791 could we shorten the treatment of mycobacterial infections? *Microb Cell* 6:105-122.
- 792 **12.** Marrakchi H, Laneelle MA, Daffe M. 2014. Mycolic acids: structures, biosynthesis,
793 and beyond. *Chem Biol* 21:67-85.
- 794 **13.** Flemming HC, Wingender J, Szewzyk U, Steinberg P, Rice SA, Kjelleberg S. 2016.
795 Biofilms: an emergent form of bacterial life. *Nat Rev Microbiol* 14:563-575.
- 796 **14.** Ojha AK, Baughn AD, Sambandan D, Hsu T, Trivelli X, Guerardel Y, Alahari A,
797 Kremer L, Jacobs WR Jr, Hatfull GF. 2008. Growth of *Mycobacterium tuberculosis*
798 biofilms containing free mycolic acids and harbouring drug-tolerant bacteria. *Mol*
799 *Microbiol* 69:164-174.

- 800 **15.** Caceres N, Vilaplana C, Prats C, Marzo E, Llopis I, Valls J, Lopez D, Cardona P-J,
801 2013. Evolution and role of corded cell aggregation in *Mycobacterium tuberculosis*
802 cultures. *Tuberculosis* 93:1-9.
- 803 **16.** Kalsum S, Braian C,¹ Koeken VACM, Raffetseder J, Lindroth M, van Crevel R, Lerm
804 M. 2017. The cording phenotype of *Mycobacterium tuberculosis* induces the
805 formation of extracellular traps in human macrophages. *Front Cell Infect Microbiol*
806 7:278.
- 807 **17.** Sani M, Houben EN, Geurtsen J, Pierson J, de Punder K, van Zon M, Wever B,
808 Piersma SR, Jiménez CR, Daffé M, Appelmelk BJ, Bitter W, van der Wel N, Peters
809 PJ. 2010. Direct visualization by cryo-EM of the mycobacterial capsular layer: a labile
810 structure containing ESX-1-secreted proteins. *PLoS Pathog* 6:e1000794.
- 811 **18.** Trivedi A, Mavi PS, Bhatt D, Kumar A. 2016. Thiol reductive stress induces cellulose-
812 anchored biofilm formation in *Mycobacterium tuberculosis*. *Nat Commun* 7:11392.
- 813 **19.** Van Wyk N, Navarro D, Blaise M, Berrin J-G, Henrissat B, Drancourt M, Kremer L.
814 2017. Characterization of a mycobacterial cellulase and its impact on biofilm- and
815 drug-induced cellulose production. *Glycobiology* 27:392–399.
- 816 **20.** Pagani TD , Guimarães ACR , Waghabi MC , Corrêa PR, Kalume DE, Berrêdo-Pinho
817 M, Degrave WM, Mendonça-Lima L. 2019. Exploring the potential role of
818 moonlighting function of the surface-associated proteins from *Mycobacterium bovis*
819 BCG Moreau and Pasteur by comparative proteomic. *Front Immunol* 10:716.
- 820 **21.** Ojha A, Anand M, Bhatt A, Kremer L, Jacobs WR, Jr., Hatfull GF. 2005. GroEL1: a
821 dedicated chaperone involved in mycolic acid biosynthesis during biofilm formation in
822 mycobacteria. *Cell* 123:861-873.

- 823 **22.** McNamara M, Tzeng S-C, Maier C, Wu M, Bermudez LE. 2013. *Proteome Sci.*
824 Surface-exposed proteins of pathogenic mycobacteria and the role of Cu-Zn
825 superoxide dismutase in macrophages and neutrophil survival. 11: 45.
- 826 **23.** McNamara, M, Tzeng S-C,, Maier C, Zhang L, Bermudez LE. 2012. Surface
827 proteome of *Mycobacterium avium* subsp. *hominissuis* during the early stages of
828 macrophage infection. *Infect Immun.* 80:1868-1880.
- 829 **24.** Wang XM, Lu C, Soetaert K, S'Heeren C, Peirs P, Lan elle MA, Lef vre P, Bifani P,
830 Content J, Daff  M, et al. 2011. Biochemical and immunological characterization of a
831 cpn60.1 knockout mutant of *Mycobacterium bovis* BCG. *Microbiology* 157:1205-
832 1219.
- 833 **25.** Bhatt A, Fujiwara N, Bhatt K, Gurcha SS, Kremer L, Chen B, Chan J, Porcelli SA,
834 Kobayashi K, Besra GS, Jacobs WM Jr. 2007. Deletion of *kasB* in *Mycobacterium*
835 *tuberculosis* causes loss of acid-fastness and subclinical latent tuberculosis in
836 immunocompetent mice. *Proc Natl Acad Sci U S A* 104:5157-5162.
- 837 **26.** Luukinen H, Hammaren MM, Vanha-Aho LM, Parikka M. 2018. Modeling tuberculosis
838 in *Mycobacterium marinum* infected adult zebrafish. *J Vis Exp* 8:58299.
- 839 **27.** Parikka M, Hammar n MM, Harjula SK, Halfpenny 754 NJ, Oksanen KE, Lahtinen
840 MJ, Pajula ET, Iivanainen A, Pesu M, R met M. 2012. *Mycobacterium marinum*
841 causes a latent infection that can be reactivated by gamma irradiation in adult
842 zebrafish. *PLoS Pathog* 8:e1002944.
- 843 **28.** Tobin DM, Ramakrishnan L. 2008. Comparative pathogenesis of *Mycobacterium*
844 *marinum* and *Mycobacterium tuberculosis*. *Cell Microbiol* 10:1027-760.
- 845 **29.** Takaki K, Davis JM, Winglee K, Ramakrishnan L. 2013. Evaluation of the
846 pathogenesis and treatment of *Mycobacterium marinum* infection in zebrafish. *Nat*
847 *Protoc* 8:1114-11124.

- 848 **30.** Chen C, Liu H, Zabad S, Rivera N, Rowin E, Hassan M, Gomez De Jesus SM, Llinás
849 Santos PS, Kravchenko K, Mikhova M, Ketterer S, Shen A, Shen S, Navas E, Horan
850 B, Raudsepp J, Jeffery C. 2021. MoonProt 3.0: an update of the moonlighting
851 proteins database. *Nucleic Acids Res* 49(D1):D368-D372.
- 852 **31.** Brauner A, Shores N, Fridman O, Balaban NQ. 2017. An Experimental framework
853 for quantifying bacterial tolerance. *Biophys J* **112**:2664-2671.
- 854 **32.** Brauner A, Fridman O, Gefen O, Balaban NQ. 2016. Distinguishing between
855 resistance, tolerance and persistence to antibiotic treatment. *Nat Rev Microbiol*
856 14:320-330.
- 857 **33.** Glickman MS, Cox JS, Jacobs WR Jr. 2000. A novel mycolic acid cyclopropane
858 synthetase is required for cording, persistence, and virulence of *Mycobacterium*
859 *tuberculosis*. *Mol Cell* 5:717-727.
- 860 **34.** Anton V, Rougé P, Daffé M. 1996. Identification of the sugars involved in
861 mycobacterial cell aggregation. *FEMS Microbiol Lett* 144:167–170.
- 862 **35.** Glickman MS, Cahill SM, Jacobs WR Jr. 2001. The *Mycobacterium tuberculosis*
863 *cmaA2* gene encodes a mycolic acid trans-cyclopropane synthetase. *J Biol Chem*
864 276:2228-33.
- 865 **36.** Warriar T, Tropis M, Werngren J, Diehl A, Gengenbacher M, Schlegel B, Schade M,
866 Oschkinat H, Daffe M, Hoffner S, Eddine AN, Kaufmann SHE. 2012. Antigen 85C
867 Inhibition restricts *Mycobacterium tuberculosis* growth through disruption of cord
868 factor biosynthesis. *Antimicrob Agents Chemother* 56:1735–1743.
- 869 **37.** Lerner TR, Queval CJ, Lai RP, Russell MRG, Fearn A, Greenwood DJ, Collinson L,
870 Wilkinson RJ, Gutierrez MG. 2020. *Mycobacterium tuberculosis* cords within
871 lymphatic endothelial cells to evade host immunity. *JCI Insight* 5:e136937.

- 872 **38.** Nagakubo T, Tahara YO, Miyata M, Nomura N, Toyofuku M. 2021. Mycolic acid-
873 containing bacteria trigger distinct types of membrane vesicles through different
874 routes. *iScience* 24:102015.
- 875 **39.** Schooling SR, and Beveridge TJ. 2006. Membrane vesicles: an overlooked
876 component of the matrices of biofilms. *J Bacteriol* 188:5945–5957.
- 877 **40.** Chiplunkar SS , Silva CA, Bermudez LE, Danelishvili L. 2019. Characterization of
878 membrane vesicles released by *Mycobacterium avium* in response to environment
879 mimicking the macrophage phagosome. *Future Microbiol* 14:293-313.
- 880 **41.** Deng LL, Humphries DE, Arbeit RD, Carlton LE, Smole SC, Carroll JD. 2005.
881 Identification of a novel peptidoglycan hydrolase CwIM in *Mycobacterium*
882 *tuberculosis*. *Biochim Biophys Acta* 1747:57-66.
- 883 **42.** Wang C, Zhang Q, Tang X, An Y, Li S, Xu H, Li Y, Wang X, Luan W, Wang Y, Liu M,
884 Yu L. 2019. Effects of CwIM on autolysis and biofilm formation in *Mycobacterium*
885 *tuberculosis* and *Mycobacterium smegmatis*. *Int J Med Microbiol* 309:73-83.
- 886 **43.** Antikainen J, Kuparinen V, Lähteenmäki K, Korhonen TK. 2007. pH-dependent
887 association of enolase and glyceraldehyde-3-phosphate dehydrogenase of
888 *Lactobacillus crispatus* with the cell wall and lipoteichoic acids. *J Bacteriol* 189:4539-
889 4543.
- 890 **44.** Kainulainen V, Loimaranta V, Pekkala A, Edelman S, Antikainen J, Kylväjä R,
891 Laaksonen M, Laakkonen L, Finne J, Korhonen TK. 2012. Glutamine synthetase and
892 glucose-6-phosphate isomerase are adhesive moonlighting proteins of *Lactobacillus*
893 *crispatus* released by epithelial cathelicidin LL-37. *J Bacteriol* 194:2509-2519.
- 894 **45.** Foulston L, Elsholz AKW, DeFrancesco AS, Losick R. 2014. The extracellular matrix
895 of *Staphylococcus aureus* biofilms comprises cytoplasmic proteins that associate with
896 the cell surface in response to decreasing pH. *mBio* 5:e01667-14.

- 897 **46.** Dengler V, Foulston L, DeFrancesco AS, Losick R. 2015. An electrostatic net model
898 for the role of extracellular DNA in biofilm formation by *Staphylococcus aureus*. *J*
899 *Bacteriol* 197:3779-3787.
- 900 **47.** Ebner P, Götz F. 2019. Bacterial excretion of cytoplasmic proteins (ECP):
901 Occurrence, mechanism, and function. *Trends Microbiol* 27:176-187.
- 902 **48.** Graf AC, Leonard A, Schäuble M, Rieckmann LM, Hoyer J, Maass S, Lalk M,
903 Becher D, Pané-Farré J, Riedel K. 2019. Virulence factors produced by
904 *Staphylococcus aureus* biofilms have a moonlighting function contributing to biofilm
905 integrity. *Mol Cell Proteomics* 18:1036-1053
- 906 **49.** Qian J, Chen R, Wang H, Zhang X. 2020. Role of the PE/PPE family in host–
907 pathogen interactions and prospects for anti-tuberculosis vaccine and diagnostic tool
908 design. *Front Cell Infect Microbiol* 10:594288.
- 909 **50.** Wang Q, Boshoff HIM, Harrison JR, Ray PC, Green SR, Wyatt PG, Barry CE 3rd.
910 2020. PE/PPE proteins mediate nutrient transport across the outer membrane of
911 *Mycobacterium tuberculosis*. *Science* 367:1147-1151.
- 912 **51.** Pietersen R-D, du Preez I, Loots DT, van Reenen N, Beukes D, Leisching G, Baker
913 B. 2020. Tween 80 induces a carbon flux rerouting in *Mycobacterium tuberculosis*. *J*
914 *Microbiol Methods* 170:105795.
- 915 **52.** Gröschel MI, Sayes F, Simeone R, Majlessi L, Brosch R. 2016. ESX secretion
916 systems: mycobacterial evolution to counter host immunity. *Nat Rev Microbiol*
917 14:677-691.
- 918 **53.** Schorey JS, Li Q, McCourt DW, Bong-Mastek M, Clark-Curtiss JE, Ratliff TL, Brown
919 EJ. 1995. A *Mycobacterium leprae* gene encoding a fibronectin binding protein is
920 used for efficient invasion of epithelial cells and Schwann cells. *Infect Immun*
921 63:2652-2657.

- 922 **54.** Fenn K, Wong CT, Darbari VC. 2020. *Mycobacterium tuberculosis* Uses Mce proteins
923 to interfere with host cell signaling. *Front Mol Biosci* 6:149.
- 924 **55.** Vinod V, Vijayrajratnam S, Vasudevan AK, Biswas R. 2020. The cell surface
925 adhesins of *Mycobacterium tuberculosis*. *Microbiol Res* 232:126392.
- 926 **56.** Delogu G, Brennan MJ. 1999. Functional domains present in the mycobacterial
927 hemagglutinin, HBHA. *J Bacteriol* 181:7464-7469.
- 928 **57.** Berge M, Pezzatti J, Gonzalez-Ruiz V, Degeorges L, Mottet-Osman G, Rudaz S,
929 Viollier PH. 2020. Bacterial cell cycle control by citrate synthase independent of
930 enzymatic activity. *Elife* 9:e52272.
- 931 **58.** Rego EH, Audette RE, Rubin EJ. 2017. Deletion of a mycobacterial divisome factor
932 collapses single-cell phenotypic heterogeneity. *Nature* 546:153-157.
- 933 **59.** Kieser KJ, Rubin EJ. 2014. How sisters grow apart: mycobacterial growth and
934 division. *Nat Rev Microbiol* 12:550-562. doi:10.1038/nrmicro3299.
- 935 **60.** Jakkala K, Ajitkumar P. 2019. Hypoxic non-replicating persistent *Mycobacterium*
936 *tuberculosis* develops thickened outer layer that helps in restricting rifampicin entry.
937 *Front Microbiol* 10:2339.
- 938 **61.** Banerjee S, Nandyala AK, Raviprasad P, Ahmed N, Hasnain SE. 2007. Iron-
939 dependent RNA-binding activity of *Mycobacterium tuberculosis* aconitase. *J Bacteriol*
940 189:4046-4052.
- 941 **62.** Rahi A, Dhiman A, Singh D, Lynn AM, Rehan M, Bhatnagar R. 2018. Exploring the
942 interaction between *Mycobacterium tuberculosis* enolase and human plasminogen
943 using computational methods and experimental techniques. *J Cell Biochem*
944 119:2408-2417.
- 945 **63.** de la Paz Santangelo M, Gest PM, Guerin ME, Coinçon M, Pham H, Ryan G, Puckett
946 SE, Spencer JS, Gonzalez-Juarrero M, Daher R, Lenaerts AJ, Schnappinger D,

- 947 Therisod M, Ehrt S, Sygusch J, Jackson M. 2011. Glycolytic and non-glycolytic
948 functions of *Mycobacterium tuberculosis* fructose-1,6-bisphosphate aldolase, an
949 essential enzyme produced by replicating and non-replicating bacilli. *J Biol Chem*
950 286:40219-40231.
- 951 **64.** Gengenbacher M, Rao SPS, Pethe K, Dick T. 2010. Nutrient-starved, non-replicating
952 *Mycobacterium tuberculosis* requires respiration, ATP synthase and isocitrate lyase
953 for maintenance of ATP homeostasis and viability. *Microbiology* 156:81-87.
- 954 **65.** Nandakumar M, Nathan C, Rhee K. 2014. Isocitrate lyase mediates broad antibiotic
955 tolerance in *Mycobacterium tuberculosis*. *Nat Commun* 5:4306.
- 956 **66.** Bhusal RP, Jiao W, Kwai BXC, Reynisson J, Collins AJ, Sperry J, Bashiri G, Leung
957 IKH. 2019. Acetyl-CoA-mediated activation of *Mycobacterium tuberculosis* isocitrate
958 lyase 2. *Nat Commun* 10:4639.
- 959 **67.** Daniel J, Maamar H, Deb C, Sirakova TD, Kolattukudy PE. 2011. *Mycobacterium*
960 *tuberculosis* uses host triacylglycerol to accumulate lipid droplets and acquires a
961 dormancy-like phenotype in lipid-loaded macrophages. *PLoS Pathog* 7:e1002093.
- 962 **68.** Maurya RK, Bharti S, Krishnan MY. 2018. Triacylglycerols: Fuelling the hibernating
963 *Mycobacterium tuberculosis*. *Front Cell Infect Microbiol* 8:450.
- 964 **69.** Pohane AA, Carr CR, Garhyan J, Swarts BM, Siegrist MS. 2021. Trehalose recycling
965 promotes energy-efficient biosynthesis of the Mycobacterial cell envelope. *mBio*
966 12:e02801-20.
- 967 **70.** Langklotz S, Narberhaus F. 2011. The *Escherichia coli* replication inhibitor CspD is
968 subject to growth-regulated degradation by the Lon protease. *Mol Microbiol* 80:1313-
969 1325.
- 970 **71.** Uppal S, Shetty DM, Jawali N. 2014. Cyclic AMP receptor protein regulates *cspD*, a
971 bacterial toxin gene, in *Escherichia coli*. *J Bacteriol* 196:1569-1577.

- 972 **72.** Spanka DT, Konzer A, Edelmann D, Berghoff BA. 2019. High-throughput proteomics
973 identifies proteins with importance to postantibiotic recovery in depolarized persister
974 cells. *Front Microbiol* 10:378.
- 975 **73.** Torrey HL, Keren I, Via LE, Lee JS, Lewis K. 2016. High persister mutants in
976 *Mycobacterium tuberculosis*. *PLoS One* 11:e0155127.
- 977 **74.** Beites T, O'Brien K, Tiwari D, Engelhart CA, Walters S, Andrews J, Yang H-J,
978 Sutphen ML, Weiner DM, Dayao EK, Zimmerman M, Prideaux B, Desai PV,
979 Masquelin T, Via LE, Dartois V, Boshoff HI, Barry CE, Ehrt S, Schnappinge D. 2019.
980 Plasticity of the *Mycobacterium tuberculosis* respiratory chain and its impact on
981 tuberculosis drug development. *Nat Commun* 10:4970.
- 982 **75.** Rao SPS, Alonso S, Rand L, Dick T, Pethe K. 2008. The protonmotive force is
983 required for maintaining ATP homeostasis and viability of hypoxic, nonreplicating
984 *Mycobacterium tuberculosis*. *Proc Natl Acad Sci U S A.* 105:11945-11950.
- 985 **76.** Cook GM, Hards K, Vilchèze C, Hartman T, Berney M. 2014. Energetics of
986 respiration and oxidative phosphorylation in mycobacteria. *Microbiol Spectr*
987 2:10.1128/microbiolspec.MGM2-0015-2013.
- 988 **77.** Ganguli G, Mukherjee U, Sonawane A. 2019. Peroxisomes and oxidative stress:
989 Their implications in the modulation of cellular immunity during Mycobacterial
990 infection. *Front Microbiol* 10:1121
- 991 **78.** Khare G, Nangpal P, Tyagi AK. 2017. 1. Differential roles of iron storage proteins in
992 maintaining the iron homeostasis in *Mycobacterium tuberculosis*. *PLoS One* 12(1):
993 e0169545.
- 994 **79.** Savijoki K, Nyman TA, Kainulainen V, Miettinen I, Siljamäki P, Fallarero A, Sandholm
995 J, Satokari R, Varmanen P. 2019. Growth mode and carbon source impact the
996 surfaceome dynamics of *Lactobacillus rhamnosus* GG. *Front Microbiol* 10:1272.

- 997 **80.** Savijoki K, Miettinen I, Nyman TA, Kortesoja M, Hanski L, Varmanen P, Fallarero A.
998 2020. Growth mode and physiological state of cells prior to biofilm formation affect
999 immune evasion and persistence of *Staphylococcus aureus*. *Microorganisms* 8:106.
- 1000 **81.** Cox J, Mann M. 2008. MaxQuant enables high peptide identification rates,
1001 individualized p.p.b.-range mass accuracies and proteome-wide protein
1002 quantification. *Nat Biotechnol* 26:1367-1372.
- 1003 **82.** Cox J, Neuhauser N, Michalski A, Scheltema RA, Olsen JV, Mann M. 2011.
1004 Andromeda: a peptide search engine integrated into the MaxQuant environment. *J*
1005 *Proteome Res* 10:1794-1805.
- 1006 **83.** Deutsch EW, Csordas A, Sun Z, Jarnuczak A, Perez-Riverol Y, Ternent T, Campbell
1007 DS, Bernal-Llinares M, Okuda S, Kawano S, Moritz RL, Carver JJ, Wang M,
1008 Ishihama Y, Bandeira N, Hermjakob H, Vizcaino JA. 2017. The ProteomeXchange
1009 consortium in 2017: supporting the cultural change in proteomics public data
1010 deposition. *Nucleic Acids Res* 45:D1100-D1106.
- 1011 **84.** Altschul SF, Gish W, Miller W, Myers EW, Lipman DJ. 1990. Basic local alignment
1012 search tool. *J Mol Biol* 215:403-410.
- 1013 **85.** Altschul SF, Madden TL, Schaffer AA, Zhang J, Zhang Z, Miller W, Lipman DJ. 1997.
1014 Gapped BLAST and PSI-BLAST: a new generation of protein database search
1015 programs. *Nucleic Acids Res* 25:3389-3402.
- 1016 **86.** Altschul SF, Wootton JC, Gertz EM, Agarwala R, Morgulis A, Schaffer AA, Yu YK.
1017 2005. Protein database searches using compositionally adjusted substitution
1018 matrices. *FEBS J* 272:5101-5109.
- 1019 **87.** Marchler-Bauer A, Bo Y, Han L, He J, Lanczycki CJ, Lu S, Chitsaz F, Derbyshire MK,
1020 Geer RC, Gonzales NR, Gwadz M, Hurwitz DI, Lu F, Marchler GH, Song JS, Thanki
1021 N, Wang Z, Yamashita RA, Zhang D, Zheng C, Geer LY, Bryant SH. 2017.

- 1022 CDD/SPARCLE: functional classification of proteins via subfamily domain
1023 architectures. *Nucleic Acids Res* 45:D200-D203.
- 1024 **88.** Ashburner M, Ball CA, Blake JA, Botstein D, Butler H, Cherry JM, Davis AP, Dolinski
1025 K, Dwight SS, Eppig JT, Harris MA, Hill DP, Issel-Tarver L, Kasarskis A, Lewis S,
1026 Matese JC, Richardson JE, Ringwald M, Rubin GM, Sherlock G. 2000. Gene
1027 ontology: tool for the unification of biology. The Gene Ontology Consortium. *Nat*
1028 *Genet* 25:25-29. doi:10.1038/75556.
- 1029 **89.** Rice P, Longden I, Bleasby A. 2000. EMBOSS: the European Molecular Biology
1030 Open Software Suite. *Trends Genet* 16:276-277. doi:10.1016/s0168-9525(00)02024-
1031 2.
- 1032 **90.** Petersen TN, Brunak S, von Heijne G, Nielsen H. 2011. SignalP 4.0: discriminating
1033 signal peptides from transmembrane regions. *Nat Methods* 8:785-786.
1034 doi:10.1038/nmeth.1701.
- 1035 **91.** Bendtsen JD, Kiemer L, Fausboll A, Brunak S. 2005. Non-classical protein secretion
1036 in bacteria. *BMC Microbiol* 5:58. doi:10.1186/1471-2180-5-58.
- 1037 **92.** Krogh A, Larsson B, von Heijne G, Sonnhammer EL. 2001. Predicting
1038 transmembrane protein topology with a hidden Markov model: application to
1039 complete genomes. *J Mol Biol* 305:567-80. doi:10.1006/jmbi.2000.4315.
- 1040 **93.** Sonnhammer EL, von Heijne G, Krogh A. 1998. A hidden Markov model for
1041 predicting transmembrane helices in protein sequences. *Proc Int Conf Intell Syst Mol*
1042 *Biol* 6:175-182. doi:10.1006/jmbi.2000.4315.
- 1043 **94.** Tyanova S, Temu T, Sinitcyn P, Carlson A, Hein MY, Geiger T, Mann M, Cox J.
1044 2016. The Perseus computational platform for comprehensive analysis of
1045 (prote)omics data. *Nat Methods* 13:731-740.

1046 **95.** Szklarczyk D, Gable AL, Lyon D, Junge A, Wyder S, Huerta-Cepas J, Simonovic M,
1047 Doncheva NT, Morris JH, Bork P, Jensen LJ, von Mering C. 2019. STRING v11:
1048 protein-protein association networks with increased coverage, supporting functional
1049 discovery in genome-wide experimental datasets. *Nucleic Acids Res* 47:D607-613

1050

1051 **LEGENDS for figures and tables**

1052 **Figure 1.** Mmr biofilms show distinct growth morphologies after two-weeks of growth.
1053 SBFs grow with lichen-like structures, whereas PBFs have a ribbon-like cords morphology,
1054 which becomes more defined with maturation (after 3 weeks). The WDeM images are
1055 maximum- intensity projections of one-, two-, and three-week-old biofilms (a) together with
1056 an image where Z-position is color-coded (b). X/Y scale bar corresponds to 10 μm and
1057 frame interval is 2 μm .

1058 **Figure 2. (A)** A workflow depicting the conditions and time points used for preparing the
1059 planktonic and biofilm cells of Mmr. Grey arrows indicate sampling time points for pellicle
1060 (PBF) and submerged (SBF) biofilms. (B) Workflow used for identification of surface
1061 proteins associated with planktonic (PL_log) cells, PBFs and SBFs. Marker proteins were
1062 identified by comparing the raw intensity data, statistically significant protein abundance
1063 changes by pairwise comparisons of the log₂ converted LFQ data and the protein co-
1064 abundance patterns by subjecting the LFQ data to imputation and z-score normalization.
1065 STRING and pathway enrichment analyses were conducted on the selected heat-map
1066 clusters and necessary phenotypic assays to validate the key proteome differences.

1067 **Figure 3.** The most significant protein abundance fold changes between the indicated cell
1068 types at selected timepoints. The log₂ transformed LFQ data was analyzed
1069 using Student's t-test with permutation-based FDR adjustment. In the first two top panels,
1070 the fold-change x 1000.

1071 **Figure 4. (A)** Comparison of relative transcript abundance for *celA1* between the Mmr-
1072 *CelA1* overexpression strain and the Mmr control strain with pTEC27 (WT). The *CelA1*
1073 overexpression levels were normalized to the expression level of *CelA1* in the WT control.
1074 The data is obtained from two technical replicates from two different bacterial clones. The
1075 bars represent the standard deviation. *CelA1* expression is normalized with the amount of
1076 Mmar DNA in each sample. **(B)** *CelA1* overexpression disrupts the biofilm development,
1077 and the formation of the subtype-specific growth morphologies. The WDeM images are
1078 maximum intensity projections of the two-week-old Mmr control biofilms (pTEC27, WT)
1079 and the Mmr-*CelA1* cultures (a), together with color-coded by Z-position images (b). Scale
1080 bars 100 μm and frame interval is 2 μm . **(C)** The MIC/MBC of rifampicin is reduced in both
1081 the PL and biofilms formed with the *CelA1* overexpressing strain compared to the Mmr
1082 control cultures (PTEC27, WT). Rifampicin was added to the liquid cultures two, four,
1083 seven and 14 days after the start of the culture. Ten μl per sample (in triplicate) was plated
1084 seven days after the addition of rifampicin and CFUs were counted seven days thereafter.
1085 100 CFU per sample was used as the cut-off limit for bacterial growth. The experiment
1086 was carried out three times. The figure shows a representative experiment. -, = no growth,
1087 + = bacterial growth , UNT= untreated

1088 **Figure 5. (A)** A PCA analysis of all detected proteins (based on LFQ intensities excluding
1089 one SBF_3w outlier) with PC1 and PC2 indicating growth mode- and time point-dependent
1090 changes. **(B)** Hierarchical clustering of proteins (complete linkage; n, 690) with significantly
1091 changed expression profiles. Color intensity: red and green indicate higher and lower
1092 protein abundances, respectively.

1093 **Figure 6. (A)** A PPI network analysis on cluster 1 proteins (Fig. 5B) with higher
1094 abundancies on SBFs between two and four weeks. No. nodes, 368; no. edges, 3256; PPI
1095 enrichment $P < 1.0\text{e-}16$. **(B)** A PPI network analysis on cluster six proteins with higher

1096 abundancies on SBFs between two days and 2 weeks. Proteins were clustered using MCL
1097 with the inflation parameter set to 4.0 (cluster 6) and 6.0 (cluster 1). No. nodes, 155; no.
1098 edges, 3024; PPI enrichment $P < 1.0e-16$. Circles indicate the most enriched protein
1099 interactions.

1100 **Figure 7.** A schematic model of the Mmr cell envelope with key protein abundance
1101 changes specific to PL, PBF and SBF cells. Colored arrows pointing up/down refer to
1102 protein abundances/abundance changes within the indicated cell sample types (green, PL;
1103 blue, PBFs; red, SBFs). MA, mycolic acids; cMAs, cyclopropanated mycolic acids;
1104 TDM/TMM, trehalose-6,6-dimycolate/trehalose monomycolate; PDIM/PGL, phthiocerol
1105 dimycoceros- ates/phenolic glycolipids. C, cytoplasm; IM, inner membrane; PP,
1106 periplasmic space; AG, arabinogalactan; PG, peptidoglycan; MM, mycomembrane; ECM,
1107 extracellular matrix.

1108 **Figure 8.** The proportion of persistent bacterial cells increases in Mmr biofilms. Time-kill
1109 curve analysis was performed by culturing biofilms from two days to two weeks and
1110 treating the bacteria with $400 \mu\text{g mL}^{-1}$ rifampicin. The killing kinetics were monitored for
1111 seven days by measuring the bioluminescence signal produced by Lux-Mmr daily. **(A)**
1112 Logarithmic growth phase planktonic and 2-week-old biofilm Mmr were treated with $400 \mu\text{g}$
1113 mL^{-1} of rifampicin. The time-kill curves of the planktonic and biofilm-associated bacteria
1114 were significantly different ($P < 0.0034$, log-rank test). The means and SEMs of three
1115 biological replicates are shown. **(B)** In biofilms, persistence increases over time and is
1116 significantly higher after one week compared to planktonic bacteria ($P = 0.0002$, log-rank
1117 test). Planktonic culture and two-day-old biofilm show similar killing curves. Means and
1118 SEMs of three biological replicates are shown. **(C)** Two-week-old PBFs and SBFs were
1119 tested separately for persistence. The two different biofilm-types show no difference in

1120 their persistence levels ($P = 0.51$, log-rank test). Means and SEMs of three biological
1121 replicates are shown.

1122

1123 SUPPLEMENTAL MATERIAL

1124 **Figure S1. (A)** Pellicle-type (PBF) and submerged (SBF) biofilms after culturing for two
1125 weeks (left) and 12 weeks (right). **(B)** Distribution of overlapping protein identifications
1126 within four replica samples from planktonic cell surfaces and biofilm-ECMs. PL_log,
1127 logarithmic planktonic cells; SBF, submerged type biofilms; PBF, pellicle type biofilms.

1128 **Figure S2. (A)** Distribution of identified proteins in terms of their predicted secretion motifs
1129 and the number of predicted TMDs. PL_log, logarithmic planktonic cells; PBF_all and
1130 SBF_all, all identified proteins from pellicle and submerged biofilm matrices, respectively.
1131 Other, proteins without any known motifs for classical or non-classical secretion. **(B)** Venn
1132 diagrams indicating the core and marker proteomes within all identifications (planktonic
1133 and biofilms) at each time point.

1134 **Figure S3. (A)** The bioluminescence-based readout of the biofilm killing assay was
1135 validated using the OD₆₀₀-method to monitor bacterial growth at varying time points of
1136 growth, showing similar killing kinetics as observed with the bioluminescence
1137 measurements of the same samples. Here, the four-day-old biofilm and two-day-old
1138 planktonic cells were treated with 200 $\mu\text{g mL}^{-1}$ rifampicin. The mean of three biological
1139 replicates of the OD₆₀₀-based assay is shown. **(B)** Mmr growth is accompanied by
1140 increased bioluminescence values in maturing biofilms without the antibiotic treatment,
1141 even at timepoints of over one week of biofilm culture. The bioluminescence was
1142 measured three times/three seconds using EnVision equipment (Perkin Elmer), and the
1143 mean of relative light units (RLUs) per one second was calculated. Means and SEMs of
1144 three biological replicates are shown.

1145 **Table S1.** List of all proteins identified on Mmr cells during different growth modes. The
1146 colored cells refer to the average (log₂) raw intensity values for proteins detected in at
1147 least two replica samples. Cells in grey, protein was not detected. PL_log, logarithmic
1148 planktonic cells; PBF, pellicle type biofilm cells; SBF, submerged type biofilm cells.

1149 **Table S2.** Proteins specific to pellicle biofilms (PBFs), submerged biofilms (SBFs) and to
1150 both biofilms that lack an identifiable counterpart on planktonic cell surfaces. Proteins
1151 detected in each replica samples are shown. Color gradient bar refers to log₂-transformed
1152 raw intensity values (avr., n ≥ 2): blue, low abundance; yellow, high abundance; PBF,
1153 pellicle biofilm; SBF, submerged biofilm.

1154 **Table S3.** Log₂-transformed MaxLFQ data with minimum of two valid identifications (out of
1155 four) in at least one group, and statistically significant protein abundance changes between
1156 the PL and PBF_2, PL and SBF-2d, PBF_2w_SBF_2d, PBF_12w and SBF_12w, PBF_4w
1157 and 12w and SBF_4w and 12w.

1158 **Table S4.** Statistically significant protein abundance changes within planktonic cell
1159 surfaces and biofilm-ECMs. Colored cells in column "Cluster" correspond to those used in
1160 the heat-map (Fig. 5). Significant changes were calculated using a multiple-sample test
1161 (ANOVA model, FDR < 0.05, S0 = 0.1). Color intensity code bar below, blue - low
1162 abundance; yellow - high abundance.

1163 **Table S5.** Functional enrichment analysis (GO, KEGG, InterPro, Pham) on cluster 1, 2 and
1164 6 proteins (Figure 5) were studied using the STRING database v. 11 with both the rank-
1165 and gene set-based approaches (FDR of 0.05).

1166 **Table S6.** Key proteome changes within the planktonic cell surfaces and biofilm matrices
1167 at different time points of growth. Gradient bar, normalized identification intensity values
1168 (avg. ≥ 3).

1169 **Table S7.** Colony ability of non-shaved and enzymatically shaved biofilm and planktonic
1170 cells. Biofilm cells were cultured for two weeks and planktonic cells for two days, as
1171 described in material and methods. Cells in three biological replicates were suspended in
1172 trypsin/Lys-C digestion buffer and then divided into two aliquots; the first aliquot was taken
1173 as the non-shaved cell control containing only the digestion buffer, and the second aliquot
1174 of cells was treated with the trypsin/Lys-C enzyme. After 20 min incubation at 37 °C, the
1175 cell suspensions were suspended gently in PBS containing 0.2% Tween80 (v/v) and
1176 serially diluted cells were spotted in four technical replicates (10 uL each) on an agar plate.
1177 After one week cultivation at 37 °C, the colonies were calculated and compared under
1178 different conditions. nd, colonies could not be counted due to the presence of cell
1179 aggregates.

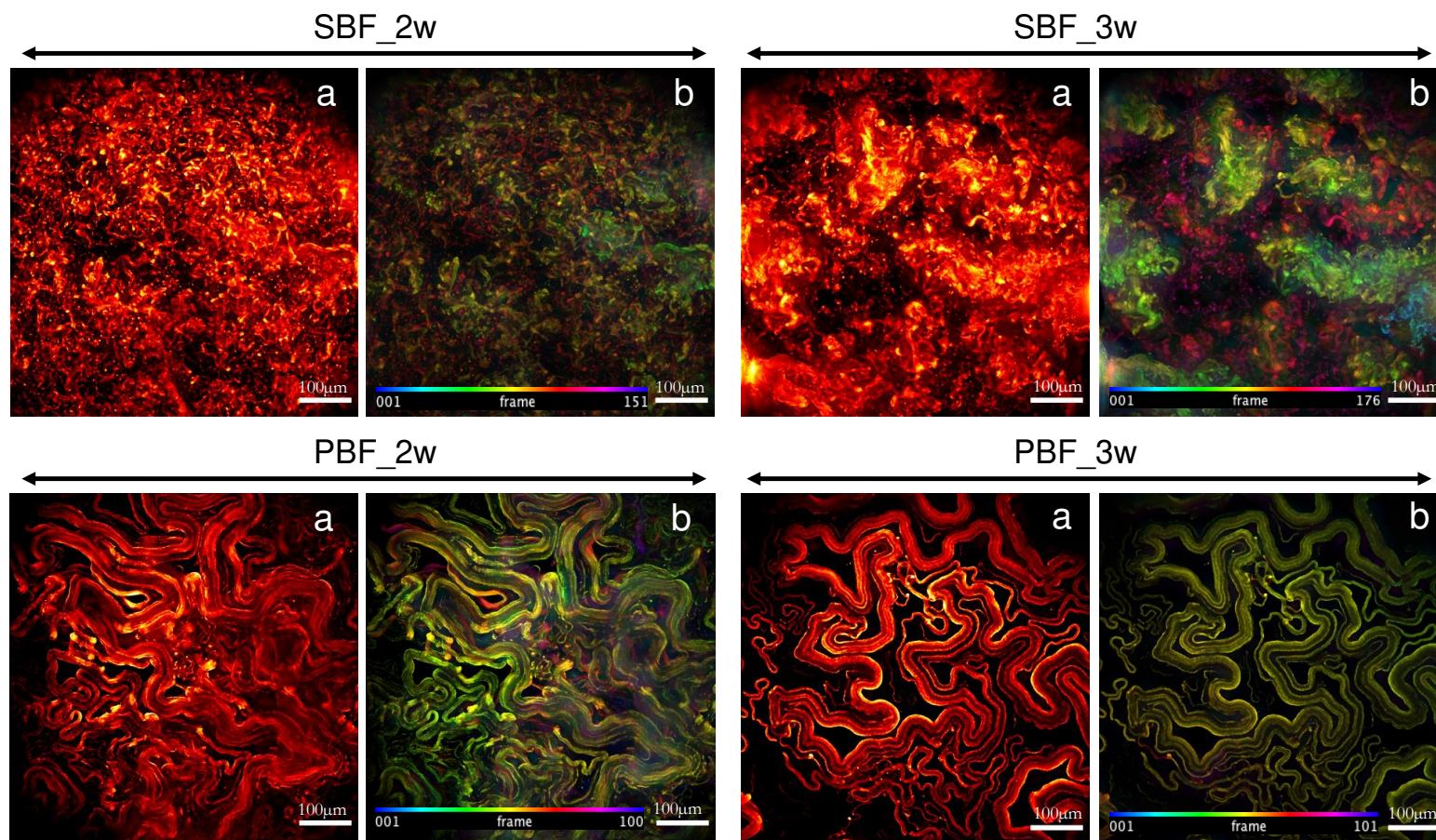
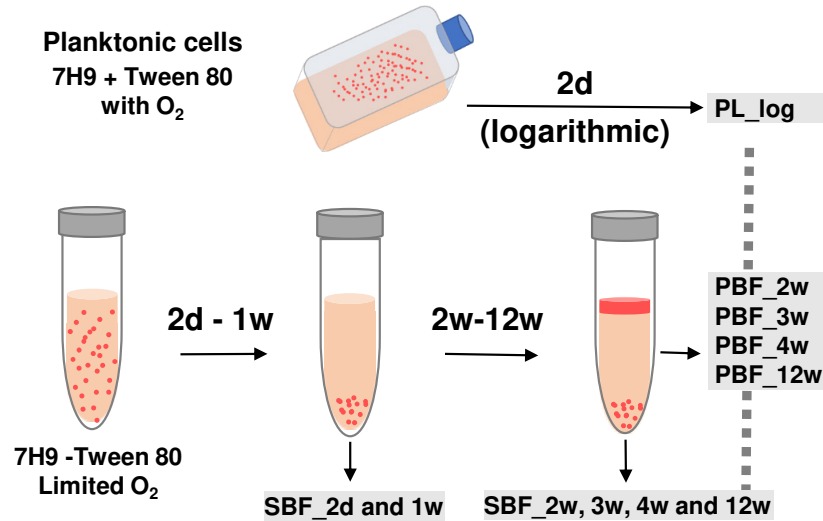


Fig. 1

Fig. 2

A



B

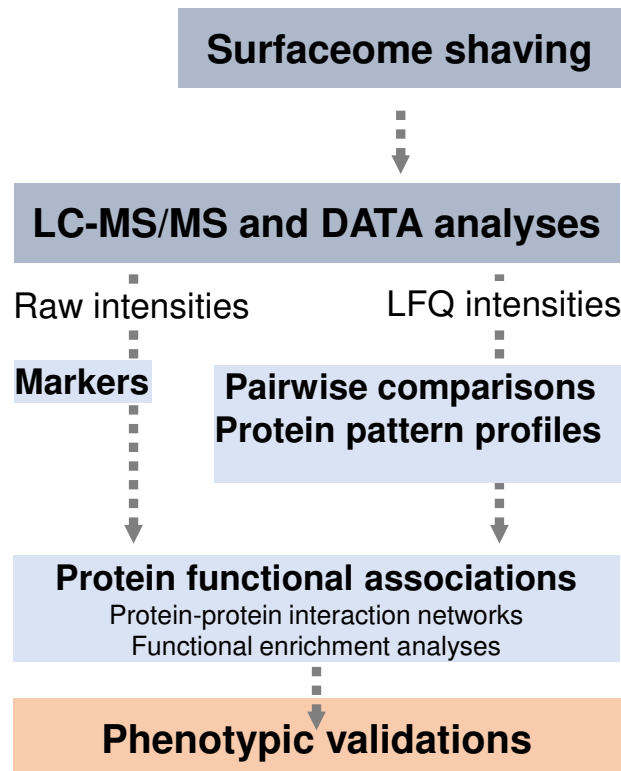


Fig. 3

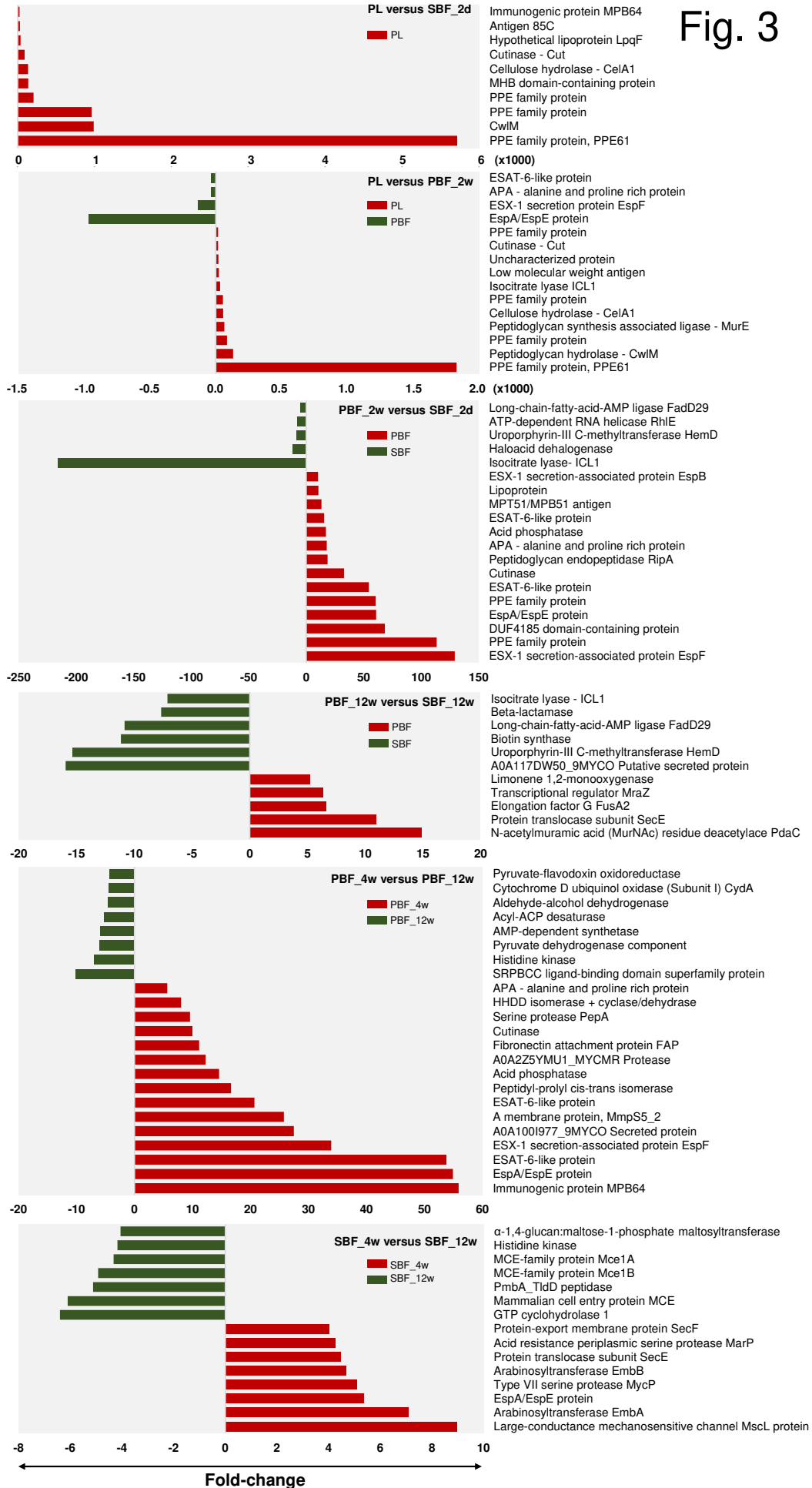
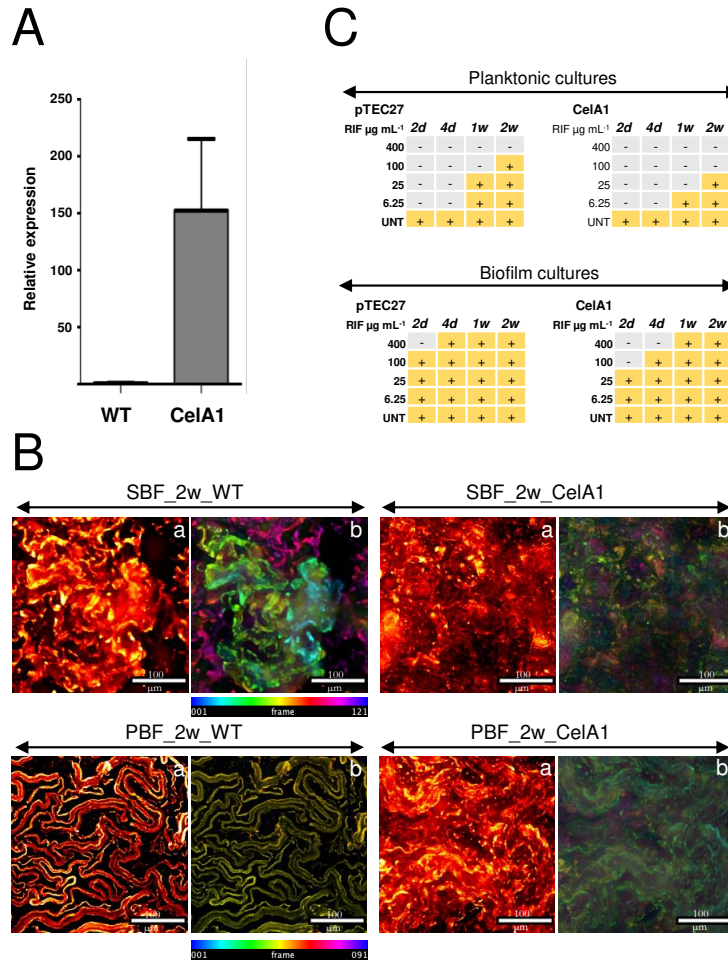


Fig. 4



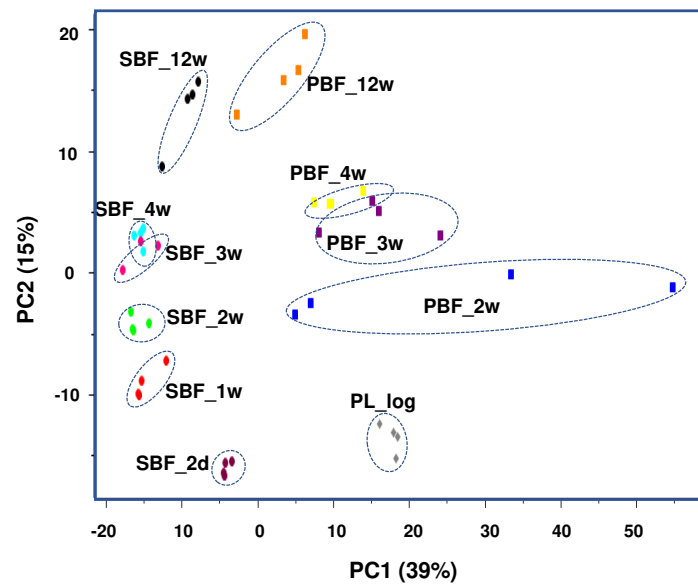
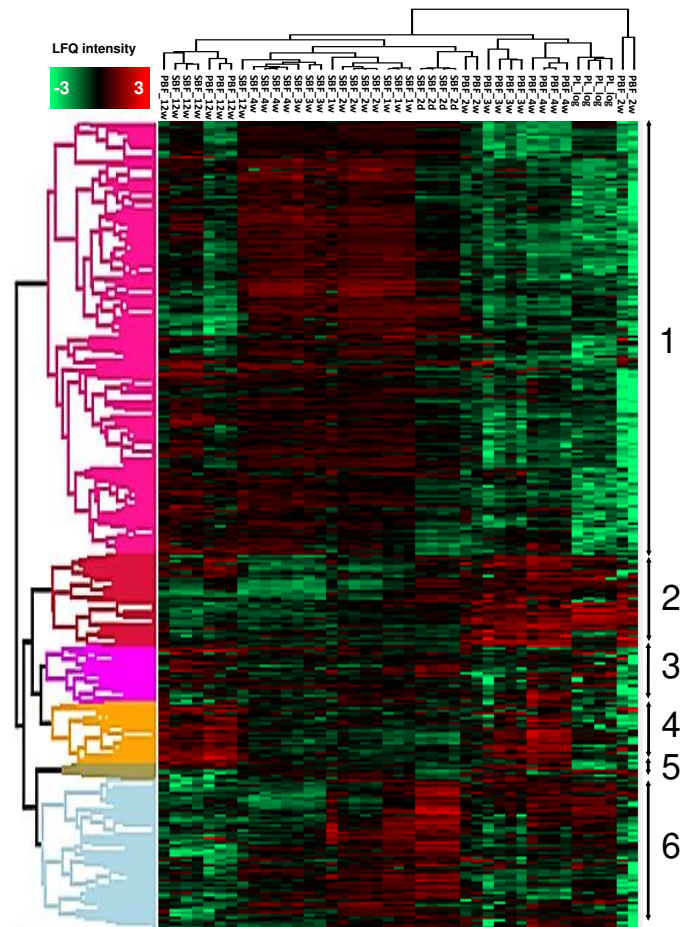
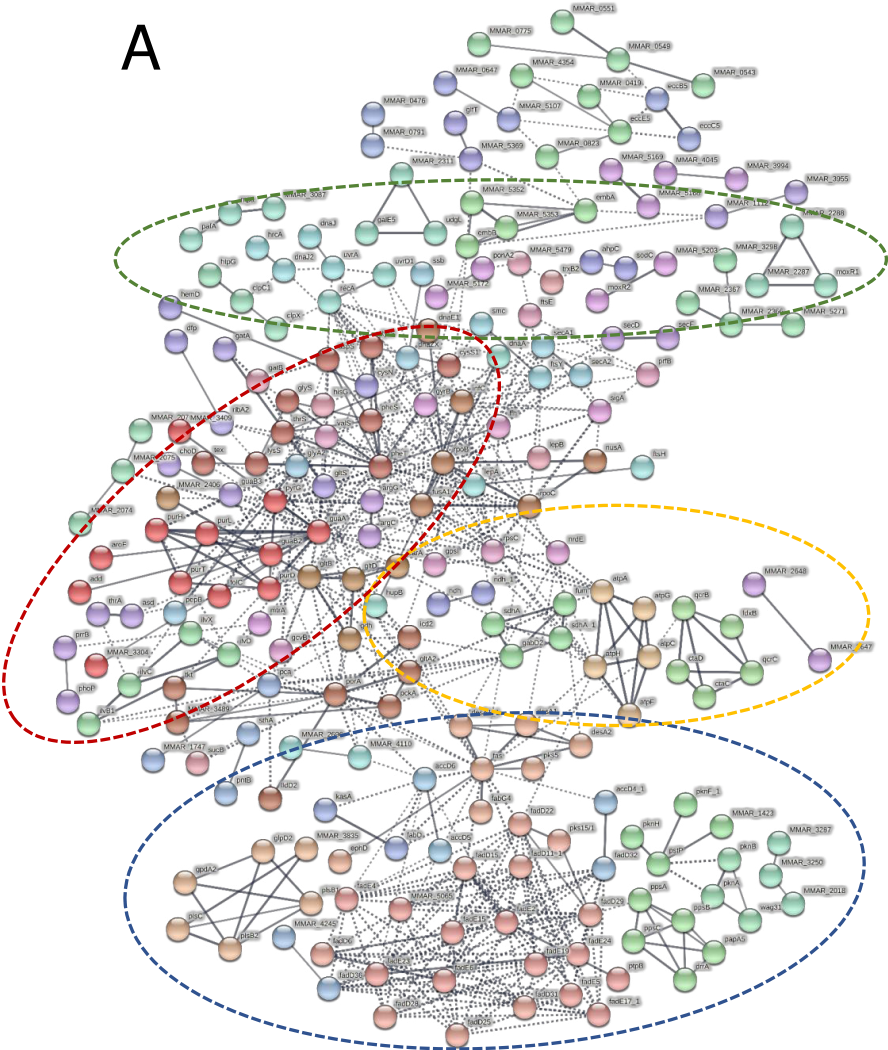
A**B**

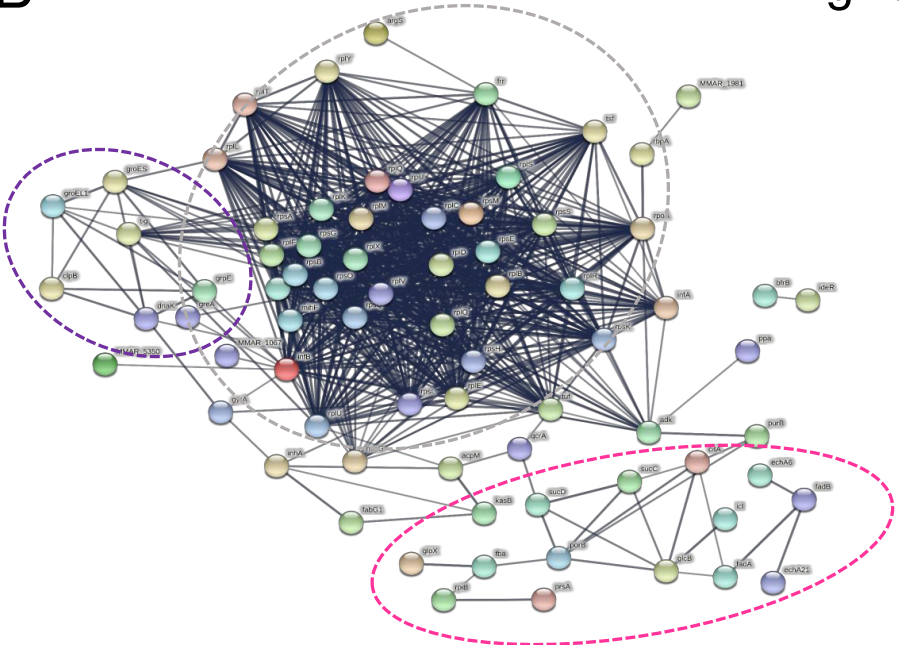
Fig. 5

Fig. 6

A



B









-  Amino acid biosynthesis
-  Stress response
-  Respiratory electron transfer and ATP synthesis
-  Fatty acid biosynthesis and aerobic β -oxidative degradation fatty acids
-  Translation (r-proteins)
-  Glycolysis and TCA cycle

Fig. 7

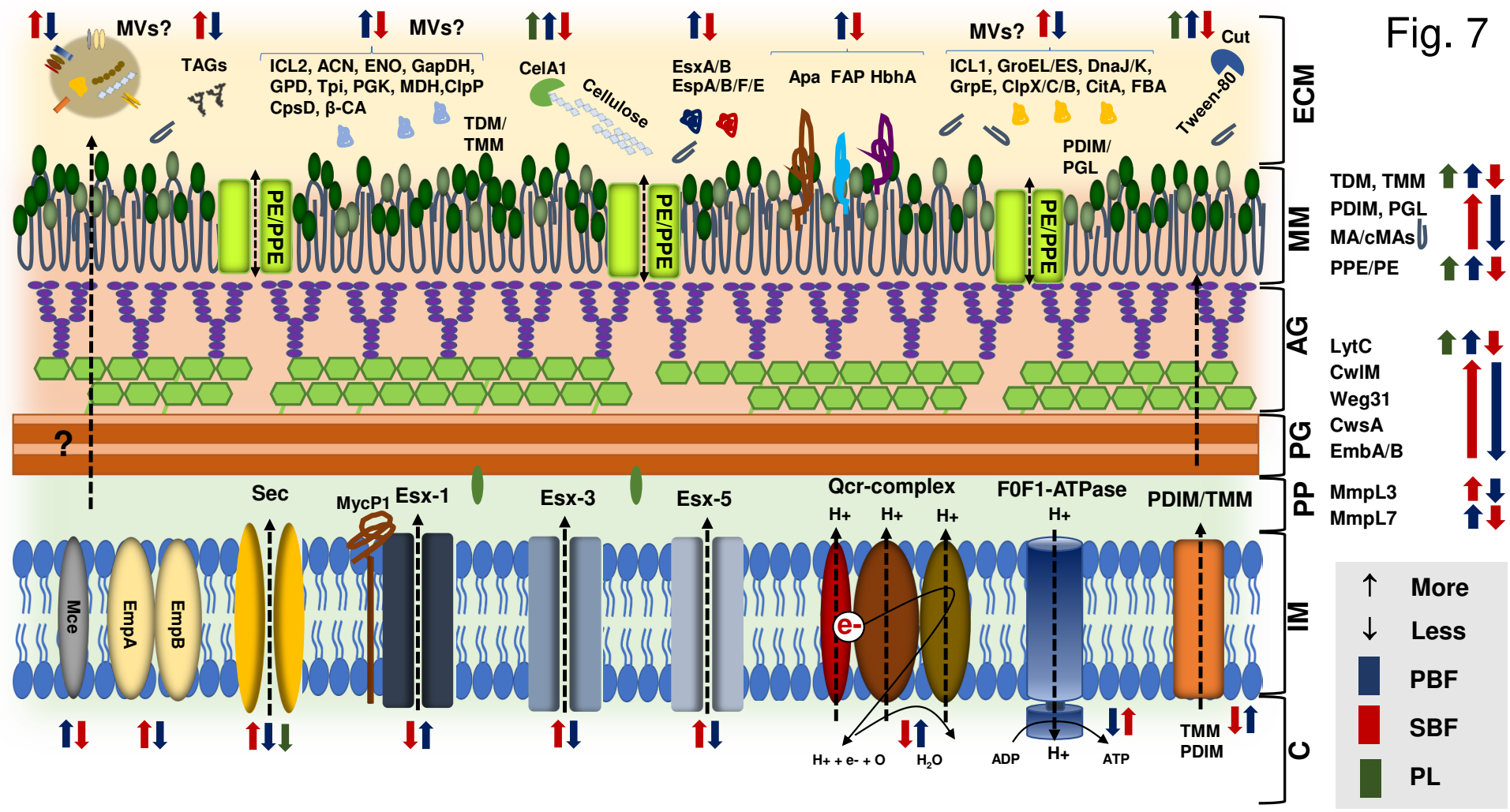
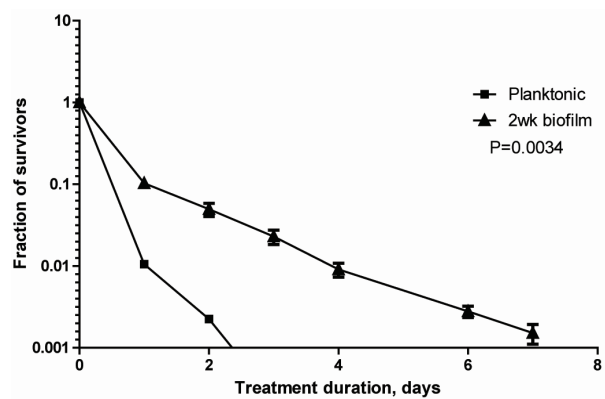
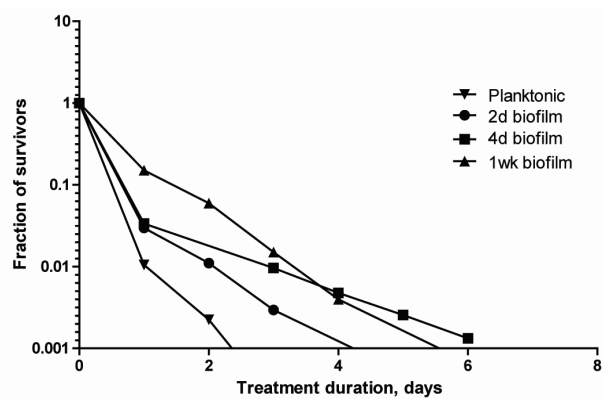


Fig. 8

A



B



C

